TU Delft Delft University of Technology

Department of Precision and Microsystems Engineering

Model Order Reduction for a Nonlinear Finite Element Model of a Joined Wing Structure

Name: Golara Riahi

Report no: EM 2012.016
Coach: dr. ir. P. Tiso
Professor: prof. ir. D.J. Rixen
Specialisation: Engineering Mechanics
Type of report: Masters Thesis
Date: Delft, July 6, 2012

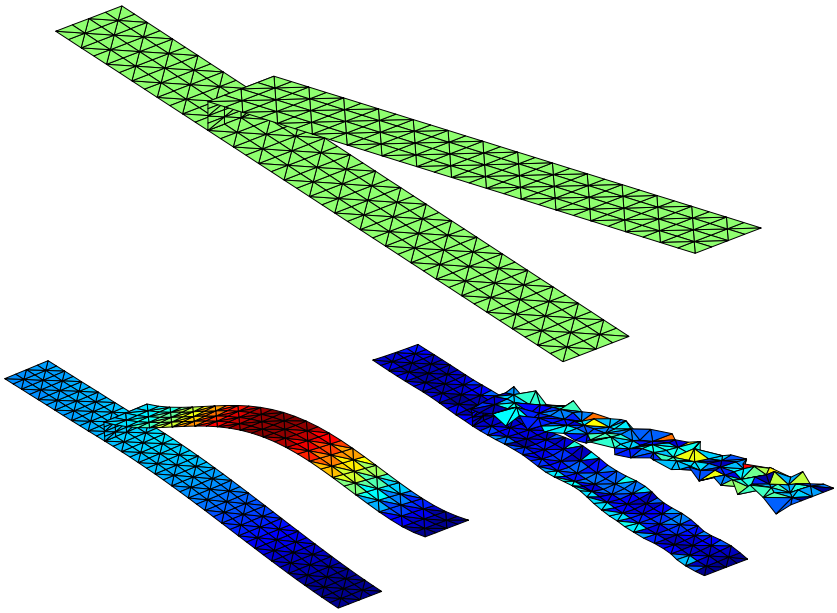

To my brother Siamak

Contents

Preface

The experiences I had in Delft has helped me not only to improve my knowledge about the world and life, but they also had a prominent influence on my personal development. I am grateful for the chances that I have been given. I hope that this thesis reflects part of what I learned in Delft, but also that other readers find it useful and interesting to read.

I would like to thank Paolo Tiso for supervising my MSc project. It is for his help and guidance that the project is completed with satisfying results and stayed interesting as well. I also want to thank Prof. Daniel Rixen for his support and supervision during my MSc studies and projects in Delft. Also for his efforts and help to find me good projects. I would like to thank Paul van Woerkom for his guidance during my studies in Delft. It was for 'Dynamica 2' that I could choose my MSc specialisation. And his efforts for me to find a MSc project with aerospace background. Well, we found it finally but from a different source!

What is 'student life' without friends and fellow student colleagues? I want to thank Nazgol, Julie, Rad, Ferry, Johann, Rob and ... for the good time we had, which made studying more joyful. I want to specially thank Medya for her precious friendship, encouragement, help and good memories we made together. Sisterhood is not easy to find, surely not in technical university, and I am grateful for it.

I would like to extend my sincere gratitude to my family specially my sister Soheila and my brother Siamak for their encouragements, support and guidance. You have always been my model in life. I hope you are happy with your little sister's achievement. Also I want to express my thankfulness to Irene for her efforts that made it possible for me to come to the Netherlands in the first place and all her help after I was here.

Finally I want to thank Stephan for all his love, support and patience. Having you by my side has helped me through this challenging time and made the good times even more joyful than I could have ever imagined.

List of Acronyms

MOR Model Order Reduction

DoF Degrees of freedom

FE finite element

JW Joined Wing

VM vibration mode

MD modal derivative

3D Three Dimensional

RBM Rigid Body Mode

FEM Finite Element Method

POD Proper Orthogonal Decomposition

SVD Singular Value Decomposition

Summary

Joined Wing is a concept of nonplanar airplane wing structure. This is a new concept which is not yet used for commercial airplanes but has proven to have several advantages such as lowering the drag and lighter weight combined with higher stiffness. It also increases the maneuverability.

However the simulation of the structure using Finite Element Method introduces too many degrees of freedom. Therefore it is necessary to reduce the system of equations using modal order reduction. The common methods of using vibration modes in a reduction basis to reduce the system, fail for nonlinear structures, as with large displacements, the vibration modes of the structure change.

Modal derivatives show how a certain mode changes in the direction of another mode. Including modal derivatives in the reduction basis improves the reduction of the model but is very much dependent on the geometry of the structure.

In this work, the reduction basis is set up using vibration modes and modal derivatives. It is investigated why this basis fails to reduce the system of the joined wing accurately. By calculating for the remainder, proper orthogonal decomposition and Krylov sequence the reduction basis is improved. Finally a greedy algorithm applied to the joined wing problem succeeds in reducing the system by finding the best possible improvement of the reduction basis for each load step.

Chapter 1

Introduction

1.1 The joined wing concept

Joined Wing (JW) is one of different concepts for nonplanar wing structures. These nonplanar wings are primarily intended to reduce drag and wingtip vortices [10] which can lead to less fuel consumption.
For an airplane with joined wings, the two wings are coupled such that the airplane has a diamond shape from top and front views. Some of the advantages that are claimed for the JW are "lighter weight and higher stiffness, higher span-efficiency factor, higher trimmed maximum lift coefficient, lower wave drag, plus built-in direct lift and direct side force control capability" which are supported by independent studies [18].
Also because of the resulting diamond shape, the JW increases the maneuverability of the airplane, which is mostly advantageous for fighter aircrafts.
However because the decrease in fuel consumption is not very high, the financial benefits of the joined wings are minor for commercial use [11].

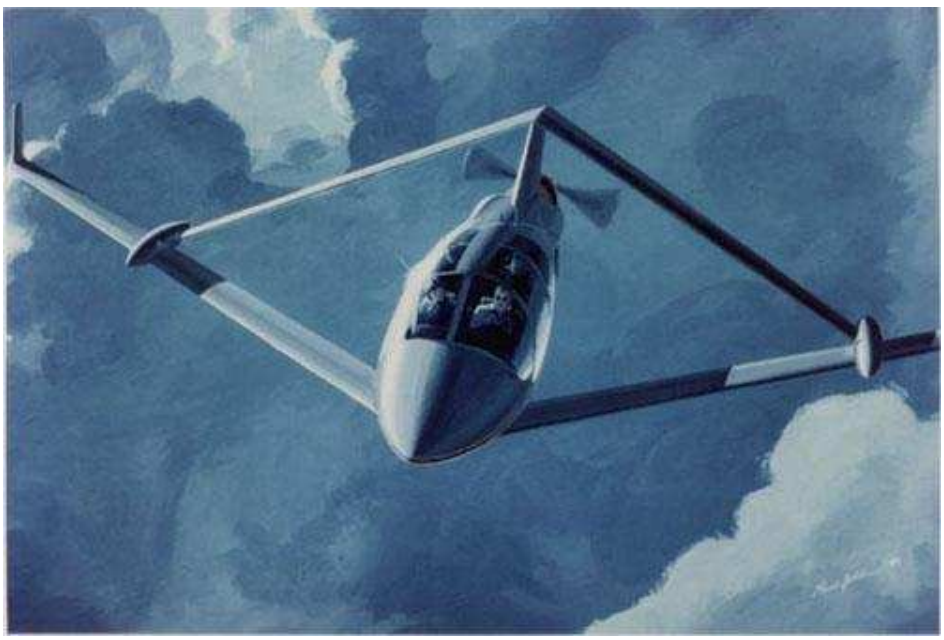

Figure 1.1: An artist impression of the JW concept [11].

1.2 Structural modeling of the JW

Before building and using such a structure as the JW, it is necessary to simulate the structure both statically and dynamically, to find its weak points and to be able to improve the structure. This includes shape optimizations and material selections. Furthermore the chosen structure must be capable of withstanding operational dynamic loads.
To simulate such a structure statically, stress equilibrium equations have to be solved which are partial differential equations, defined on a complicated geometry. The dynamic extension of these equations are the equations of motion.
Finite Element Method (FEM) is a numerical method to approximate the solutions of the continuous partial differential equations. With this method the physical domain is divided into subdomains called elements. On these elements the solution is described by discrete nodal displacements and their admissible deformations known as shape functions. This approach can be popularly described as 'divide and conquer'. A disadvantage of FEM is however that each element has several nodes, therefore a FEM model has a large amount of degrees of freedom. This makes solving a FEM model computationally expensive, especially if the model is nonlinear.
No phenomenon in nature is linear! But to be able to live and build, mankind can smartly think of circumstances and assumptions to describe a phenomenon with linear equations, with other words the nonlinear effects are assumed small enough to be neglected.
We can assume for example that a pendulum moves linearly, but that would be only valid when it moves under a small angle, less than 6° to be precise. Then the equations of motion can be linearized for the pendulum. So we can predict the displacement of the pendulum as a function of time with linear equations. But as this angle grows, the linearized equations of motion are not sufficient to predict the location of the pendulum.
A case where the nonlinearities need to be considered is when the nonlinear effects have a crucial influence on the structural stability, strength, deflection, etc. of the design. This is potential the case for the JW concept.

1.3 Model Order Reduction

It has been mentioned that the Finite Element Method is a suitable approach to model the structural strength of the JW. However the FEM models are large (a lot of nodal degrees of freedom) and therefore slow to solve on a computer.
One approach to solve big FEM models is to use Model Order Reduction (MOR) [7]. In that case the number of ways that the model can move and deform is restricted to a certain set of shapes. It is crucial that this set of shapes allows for enough flexibility to correctly model the motion of a FEM model.

1.4 MOR fails for the JW

Model order reduction is especially difficult for nonlinear models (e.g. [8]). One reason is that a set of shapes that is flexible enough for linear models can be too restrictive for nonlinear models. For a linear system, by increasing the amplitude of the external force

(and not changing its shape) on the structure, the displacement amplitude increases but the displacement shapes do not change; while for a nonlinear structure, also the shapes of the displacements change. Therefore several methods to enhance the sets of shapes have been developed [5, 14, 15].
This is especially the case for the JW model for which many enhancement methods that work for other nonlinear problems do not work.

1.5 Goal and lay-out of this report

Goal of this project is to find out why the enhancement methods that work for other nonlinear problems do not work for the JW and find directions to obtain enhancement methods that do work for the JW problem.
Therefore in chapter 2 the theory behind the nonlinear FEM model of the JW is discussed as well as the basics of Model Order Reduction.
In chapter 3 an overview of methods in literature for nonlinear MOR in general an MOR for JW specifically is given.
Thereafter in chapter 4 the structure of the JW is simplified and the methods introduced in previous chapter are tested on the JW problem to improve MOR for JW. The simpler cantilever and c-shape problems that were defined to test specific aspects of the reduction methods.
The most interesting phenomena from chapter 4 are discussed in chapter 5.
Finally the conclusions and recommendations are presented in 6.

Chapter 2

Theory of Geometrically Nonlinear Mechanics

The JW is a thin-walled structure which is modeled as a shell finite element model. The uniform pressure that the JW is exposed to, results in a nonlinear response. Therefore before reducing the equilibrium equations a well understanding of the nonlinear mechanical model is needed. The material behaviour is assumed to be linear elastic (Hooke's law) and it is assumed that the nonlinearity is caused only by a nonlinear strain-displacement relation (geometric nonlinearity).
The kinematic relations for plates are explained and then extended for plates modeled with FEM. The material relations are then defined. The static equilibrium of the structure is found with the help of the principle of virtual work and nonlinear equilibrium equations are solved. After assembling the equations of motion, the eigenmodes of the structure are found which form a reduction basis with the modal derivatives.
Matlab is used to model the problem and the physical relations programmed in Matlab are verified using Ansys.

2.1 Kinematic relations for shells

A shell is a Three Dimensional (3D) solid structure with a small thickness dimension (h), compared to its surface dimension. For a shell the kinematic relations can be written using the von Karman equations. In that case the strains are [15].

$$\epsilon_x = \frac{\partial u}{\partial x} + \frac{1}{2}\left(\frac{\partial w}{\partial x}\right)^2 \tag{2.1}$$

$$\epsilon_y = \frac{\partial v}{\partial y} + \frac{1}{2}\left(\frac{\partial w}{\partial y}\right)^2 \tag{2.2}$$

$$\epsilon_{xy} = \frac{1}{2}\left(\frac{\partial u}{\partial y} + \frac{\partial v}{\partial x}\right) + \frac{1}{2}\left(\frac{\partial w}{\partial x}\frac{\partial w}{\partial y}\right) \tag{2.3}$$

where u, v and w denote the displacement in x, y and z directions respectively. These variables are depicted in figure 2.1. However these equations neglect terms in the order of $\left(\frac{\partial u}{\partial x}\right)^2$, which means that nonlinear rotations are neglected. Therefore the simplified

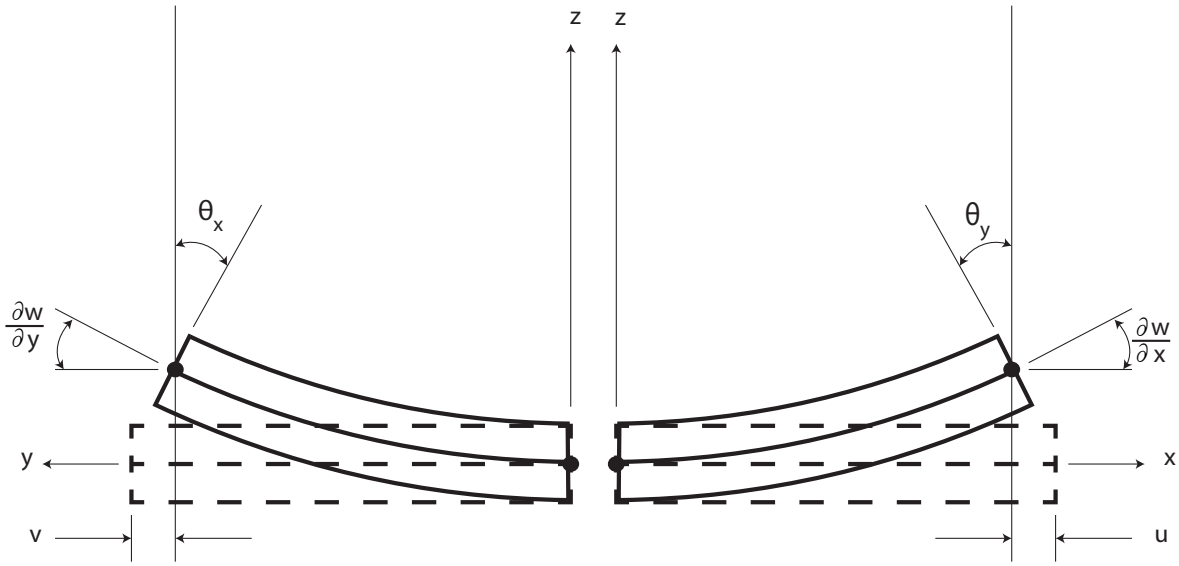

Figure 2.1: An element of the thin shell of JW in bending [6].

material strain tensor of Green-Lagrange will be used for strain measures

$$\epsilon_x = \frac{\partial u}{\partial x} + \frac{1}{2}\left(\frac{\partial v}{\partial x}\right)^2 + \frac{1}{2}\left(\frac{\partial w}{\partial x}\right)^2 \tag{2.4}$$

$$\epsilon_y = \frac{\partial v}{\partial y} + \frac{1}{2}\left(\frac{\partial u}{\partial y}\right)^2 + \frac{1}{2}\left(\frac{\partial w}{\partial y}\right)^2 \tag{2.5}$$

$$\epsilon_{xy} = \frac{1}{2}\left(\frac{\partial u}{\partial y} + \frac{\partial v}{\partial x}\right) + \frac{1}{2}\left(\frac{\partial w}{\partial x}\frac{\partial w}{\partial y}\right) \tag{2.6}$$

2.1.1 FEM version of the kinematic relation

Having evaluated the differential equations for the continuous physical model, the structure is now discretised to be evaluated numerically. In this discretisation, the domain (surface) is divided into a finite number of sub-domains called elements by means of nodes [6]. For each node of the structure a displacement vector is defined [15]

$$\mathbf{u}_s = \begin{bmatrix} u_s \\ v_s \\ w_s \\ \theta_{x_s} \\ \theta_{y_s} \\ \theta_{z_s} \end{bmatrix} \qquad s = 1 \dots N \tag{2.7}$$

where θ_{x_s}, θ_{y_s} and θ_{z_s} define the rotations around x, y and z axis respectively [1] (figure 2.1). This gives every node i six Degrees of freedom (DoF) in the 3D space. JW is meshed with simplex elements, so each three nodes form an element. In that case the elemental DoF can be written as

$$\mathbf{u}^e = \begin{bmatrix} \mathbf{u}_1 \\ \mathbf{u}_2 \\ \mathbf{u}_3 \end{bmatrix} \tag{2.8}$$

The displacement of an element is approximated by the shape functions. Shape

[1] A point in a 3D continuum, does not have rotations, but in a plate FEM, a point (node) defines a cross section (thickness h) and the rotations belong to this cross section.

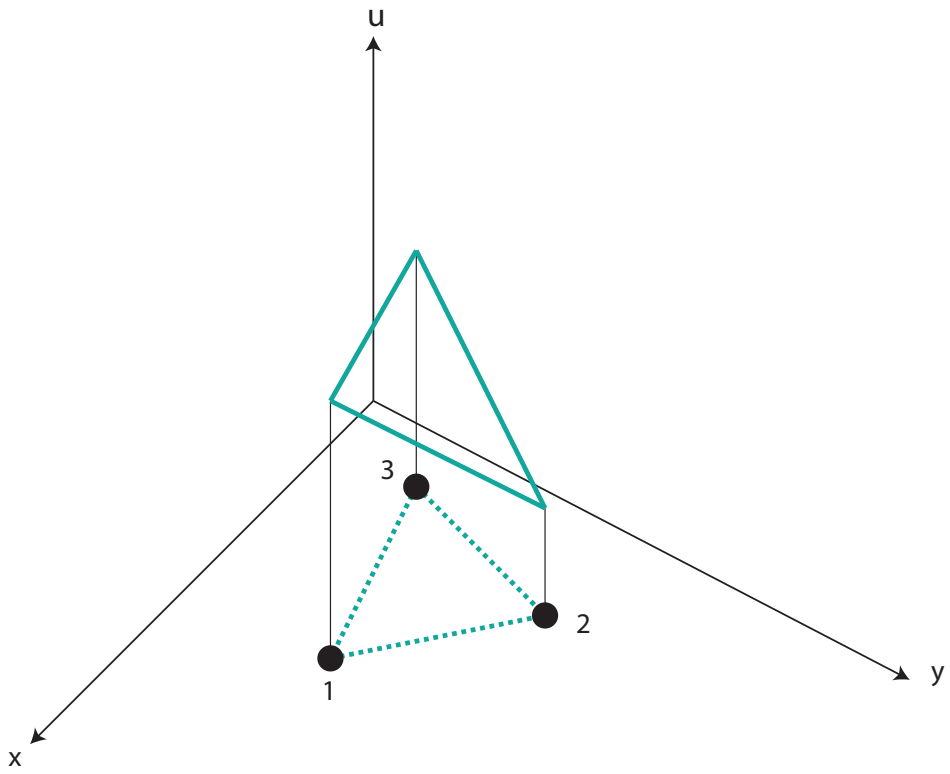

Figure 2.2: Displacement of simplex element [6].

functions are functions that are used to describe the allowable displacements. It is assumed that the continuous displacement field can be written as a superposition of shape functions times nodal displacements. Figure 2.2 shows a simplex element before (dashed) and after (solid) deformation and displacement. The standard interpolation function to find the approximation to DoF u is

$$u(x, y) = a + bx + cy \tag{2.9}$$

which consists of the values for each node 1, 2 and 3

$$u(x_1, y_1) = u_1 = a + bx_1 + cy_1 \tag{2.10}$$
$$u(x_2, y_2) = u_2 = a + bx_2 + cy_2 \tag{2.11}$$
$$u(x_1, y_3) = u_3 = a + bx_3 + cy_3 \tag{2.12}$$

With these three equations, the three unknowns a, b and c can be found. After substitution in equations 2.10, we find that

$$u = \zeta_1(x, y)u_1 + \zeta_2(x, y)u_2 + \zeta_3(x, y)u_3 \tag{2.13}$$

with

$$\zeta_1(x, y) = \frac{1}{2A}[(x_2y_3 - x_3y_2) + (y_2 - y_3)x + (x_3 - x_2)y] \tag{2.14}$$
$$\zeta_2(x, y) = \frac{1}{2A}[(x_3y_1 - x_1y_3) + (y_3 - y_1)x + (x_1 - x_3)y] \tag{2.15}$$
$$\zeta_3(x, y) = \frac{1}{2A}[(x_1y_2 - x_2y_1) + (y_1 - y_2)x + (x_2 - x_1)y] \tag{2.16}$$

where A is the surface area of each element

$$A = \frac{y_{12}x_{13} - x_{12}y_{13}}{2} \tag{2.17}$$

with $x_{ij} = x_i - x_j$ and $y_{ij} = y_i - y_j$, $i, j = 1 \dots 3$. Each shape function ζ_i, $i = 1 \dots 3$, has the value 1 at u_j, $j = 1 \dots 3$, when $i = j$ and zero otherwise, so also the sum of the shape functions for an element is 1.

$$\zeta_1 + \zeta_2 + \zeta_3 = 1 \tag{2.18}$$

This can be used to discretise the displacement field

$$\begin{bmatrix} u(x,y) \\ v(x,y) \\ w(x,y) \\ \theta_x(x,y) \\ \theta_y(x,y) \\ \theta_z(x,y) \end{bmatrix} = \boldsymbol{\zeta}\mathbf{u}^e \tag{2.19}$$

where $\boldsymbol{\zeta}$ is a $[6 \times 18]$ sized matrix containing the element shape functions and $\mathbf{u}^e$ is the vector with nodal displacements of an element which is $[18 \times 1]$. The shape function derivatives are used to describe the FEM discretization of the simplified Green-Lagrange strains (2.4) as

$$\boldsymbol{\epsilon} = \mathbf{B}\mathbf{u} + \frac{1}{2}\mathbf{C}(\mathbf{u})\mathbf{u} \tag{2.20}$$

where $\mathbf{B}$ is a constant matrix containing shape function derivatives and $\mathbf{C}(\mathbf{u})$ is a matrix that is linear in $\mathbf{u}$. The matrix $\mathbf{B}$ can be written as

$$\mathbf{B} = \begin{bmatrix} \mathbf{B}_1 & \mathbf{B}_2 & \mathbf{B}_3 \end{bmatrix} \tag{2.21}$$

where

$$\mathbf{B}_1 = \begin{bmatrix} y_{23} & 0 & & x_{32} \\ 0 & x_{32} & [0]_{3\times3} & y_{23} \\ \frac{y_{23}(y_{13}-y_{21})}{6} & \frac{x_{32}(x_{31}-x_{12})}{6} & & \frac{(x_{31}y_{13}-x_{12}y_{21})}{6} \end{bmatrix} \tag{2.22}$$

$$\mathbf{B}_2 = \begin{bmatrix} y_{31} & 0 & & x_{13} \\ 0 & x_{13} & [0]_{3\times3} & y_{31} \\ \frac{y_{31}(y_{21}-y_{32})}{6} & \frac{x_{13}(x_{12}-x_{23})}{6} & & \frac{(x_{12}y_{21}-x_{23}y_{32})}{6} \end{bmatrix} \tag{2.23}$$

$$\mathbf{B}_3 = \begin{bmatrix} y_{12} & 0 & & x_{21} \\ 0 & x_{21} & [0]_{3\times3} & y_{12} \\ \frac{y_{12}(y_{32}-y_{13})}{6} & \frac{x_{21}(x_{23}-x_{31})}{6} & & \frac{(x_{23}y_{32}-x_{31}y_{13})}{6} \end{bmatrix} \tag{2.24}$$

and the term $1/2\mathbf{C}(\mathbf{u})\mathbf{u}$ defines the quadratic relation between nodal displacements and strain where matrix $\mathbf{C}(\mathbf{u})$ is linear in $\mathbf{u}$ and is equal to

$$\mathbf{C} = \begin{bmatrix} \mathbf{u}^T\mathbf{K}_{xx} \\ \mathbf{u}^T\mathbf{K}_{yy} \\ \mathbf{u}^T\mathbf{K}_{xy} \end{bmatrix} \tag{2.25}$$

where $\mathbf{K}_{xx}$, $\mathbf{K}_{yy}$ and $\mathbf{K}_{xy}$ are geometric stiffness matrices corresponding to the stiffness of the element in the denoted directions

$$\mathbf{K}_{xx} = \mathbf{B}_w^T \mathbf{T}_x^T \mathbf{T}_x \mathbf{B}_w + \mathbf{B}_v^T \mathbf{T}_x^T \mathbf{T}_x \mathbf{B}_v \tag{2.26}$$
$$\mathbf{K}_{yy} = \mathbf{B}_w^T \mathbf{T}_y^T \mathbf{T}_y \mathbf{B}_w + \mathbf{B}_u^T \mathbf{T}_y^T \mathbf{T}_y \mathbf{B}_u \tag{2.27}$$
$$\mathbf{K}_{xy} = \mathbf{B}_v^T \left(\mathbf{T}_x^T \mathbf{T}_y + \mathbf{T}_y^T \mathbf{T}_x \right) \mathbf{B}_u \tag{2.28}$$

where the matrices $\mathbf{B}_u$, $\mathbf{B}_v$ and $\mathbf{B}_w$ are expansion matrices to assign the derivatives in $\mathbf{T}$ to the corresponding DoFs u, v and w with dimensions $[3 \times 18]$. Their entries are equal to zero except for the following

$$B_{u_{1,1}} = 1 \tag{2.29}$$
$$B_{u_{2,7}} = 1 \tag{2.30}$$
$$B_{u_{3,13}} = 1 \tag{2.31}$$
$$B_{v_{1,2}} = 1 \tag{2.32}$$
$$B_{v_{2,8}} = 1 \tag{2.33}$$
$$B_{v_{3,14}} = 1 \tag{2.34}$$
$$B_{w_{1,3}} = 1 \tag{2.35}$$
$$B_{w_{2,9}} = 1 \tag{2.36}$$
$$B_{w_{3,15}} = 1 \tag{2.37}$$

and $\mathbf{T}_x$ and $\mathbf{T}_y$ are row matrices containing the derivatives of the shape functions in x and y directions

$$\mathbf{T}_x = \tfrac{1}{2A} \begin{bmatrix} y_{23} & y_{31} & y_{12} \end{bmatrix} \tag{2.38}$$
$$\mathbf{T}_y = \tfrac{1}{2A} \begin{bmatrix} x_{32} & x_{13} & x_{21} \end{bmatrix} \tag{2.39}$$

2.2 Constitutive relations

The relation between stress and strain is assumed to be linear, therefore following Hooke's law

$$\boldsymbol{\sigma} = \mathbf{D}\boldsymbol{\epsilon} \tag{2.40}$$

where $\mathbf{D}$ is a set of elastic constants which for plates can be written as

$$\mathbf{D} = \frac{Eh}{1-\nu^2} \begin{bmatrix} 1 & \nu & 0 \\ \nu & 1 & 0 \\ 0 & 0 & \frac{1-\nu}{2} \end{bmatrix} \tag{2.41}$$

where h is the thickness of the shell.

2.3 Equilibrium equation

2.3.1 Applying the virtual work principle

The static equilibrium equation can be found by applying the principle of virtual work [12]. Following this principle, the equilibrium is found when a change caused by

a virtual displacement of the external force is compensated by an equal internal energy change caused by a virtual strain.

$$\delta\boldsymbol{\epsilon}^T\boldsymbol{\sigma} = \delta\mathbf{u}^T\mathbf{f}_{ext} \tag{2.42}$$

The virtual strain is defined as follows

$$\delta\boldsymbol{\epsilon} = \frac{\partial\boldsymbol{\epsilon}}{\partial\mathbf{u}}\delta\mathbf{u} \tag{2.43}$$

Using the kinematic relation 2.20

$$\boldsymbol{\epsilon} = \mathbf{B}\mathbf{u} + \frac{1}{2}\mathbf{C}(\mathbf{u})\mathbf{u} = \left[\mathbf{B} + \frac{1}{2}\mathbf{C}(\mathbf{u})\right]\mathbf{u} \tag{2.44}$$

the virtual strain $\delta\boldsymbol{\epsilon}$ is equal to

$$\delta\boldsymbol{\epsilon} = \left[\mathbf{B} + \mathbf{C}(\mathbf{u})\right]\delta\mathbf{u} \tag{2.45}$$

and the constitutive relation 2.40 is

$$\boldsymbol{\sigma} = \mathbf{D}\boldsymbol{\epsilon} = \mathbf{D}\left[\mathbf{B}\mathbf{u} + \frac{1}{2}\mathbf{C}(\mathbf{u})\mathbf{u}\right] \tag{2.46}$$

Using the above information, the virtual work equation 2.42 becomes

$$\delta\mathbf{u}^T\left[\mathbf{B}^T + \mathbf{C}^T(\mathbf{u})\right]\mathbf{D}\left[\mathbf{B}\mathbf{u} + \frac{1}{2}\mathbf{C}(\mathbf{u})\mathbf{u}\right] = \delta\mathbf{u}^T\mathbf{f}_{ext} \tag{2.47}$$

which has to be valid for any $\delta\mathbf{u}$, therefore

$$\mathbf{B}^T\mathbf{D}\mathbf{B}\mathbf{u} + \frac{1}{2}\mathbf{B}^T\mathbf{D}\mathbf{C}(\mathbf{u})\mathbf{u} + \mathbf{C}^T(\mathbf{u})\mathbf{D}\left[\mathbf{B}\mathbf{u} + \frac{1}{2}\mathbf{C}(\mathbf{u})\mathbf{u}\right] = \mathbf{f}_{ext} \tag{2.48}$$

where the first term $\mathbf{B}^T\mathbf{D}\mathbf{B}$ is known as the linear stiffness matrix $\mathbf{K}_{lin}$ which is the stiffness matrix at zero displacement (figure 2.3). The complete equation can also be written as

$$\mathbf{f}_{int}(\mathbf{u}) = \mathbf{f}_{ext} \tag{2.49}$$

which is an N long set equations of N unknowns.
The tangent stiffness matrix $\mathbf{K}_{tan}$ is defined as follows

$$\mathbf{K}_{tan} = \frac{\partial\mathbf{f}_{int}}{\partial\mathbf{u}} = \mathbf{B}^T\mathbf{D}\mathbf{B} + \frac{1}{2}\mathbf{B}^T\mathbf{D}\mathbf{C}(\mathbf{u}) + \frac{\partial}{\partial\mathbf{u}}\left(\mathbf{C}(\mathbf{u})\mathbf{D}\left[\mathbf{B}\mathbf{u} + \mathbf{C}(\mathbf{u})\mathbf{u}\right]\right) \tag{2.50}$$

The relation between linear and tangent stiffness matrix is as follows

$$\mathbf{K}_{tan} = \mathbf{K}_{lin} + \text{higher order terms} \qquad \mathbf{K}_{tan}(\mathbf{u} = 0) = \mathbf{K}_{lin} \tag{2.51}$$

Both the linear and the tangent stiffness matrices are $[N \times N]$ sized matrices.

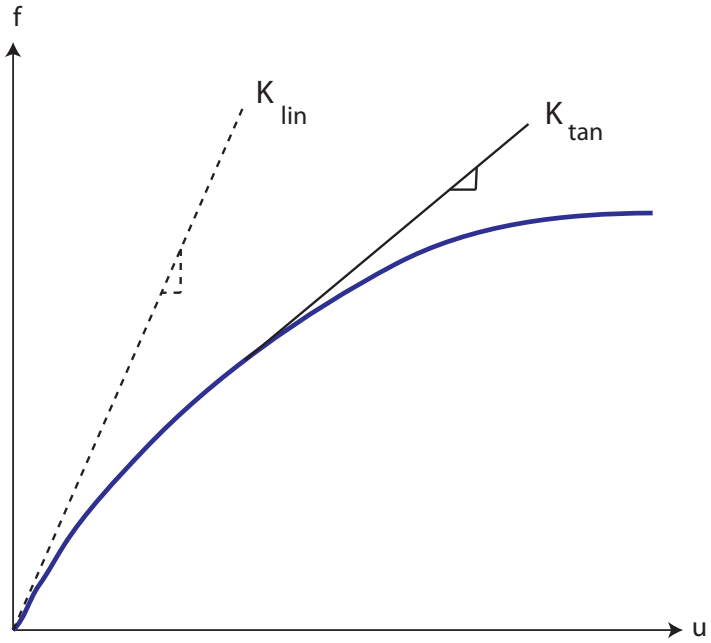

Figure 2.3: Illustration of $\mathbf{K}_{lin}$ and $\mathbf{K}_{tan}$.

2.3.2 Solving the nonlinear equilibrium equation

The nonlinear equation has to be solved by an iterative procedure. One such iterative procedure is the Newton-Algorithm [1]. Here the external load is divided in several increments. At each increment the associated displacement value to that load step is calculated in an iterative process. At each load step (increment) the following iteration procedure happens:

1. Guess an $\mathbf{u}_0$: a displacement is guessed for the corresponding load increment.
2. Compute $\mathbf{f}_{int}(\mathbf{u}_0)$: to check this guess, the internal force of this displacement is calculated.
3. Compute error $\Delta\mathbf{f} = \mathbf{f}_{ext} - \mathbf{f}_{int}(\mathbf{u}_0)$: for the system to be in equilibrium, the internal force which is calculated in the previous step must be equal to the external force.
4. Compute displacement update $\Delta\mathbf{u} = -\mathbf{K}_{tan}^{-1}\Delta\mathbf{f}$: if $\Delta\mathbf{f}$ is not small enough, the guessed displacement is not correct, the missing piece of the displacement, is calculated with the $\mathbf{K}_{tan}$ (corresponding to the internal force and the displacement) and $\Delta\mathbf{f}$.
5. Update displacements $\mathbf{u}_1 = \mathbf{u}_0 + \Delta\mathbf{u}$: a new displacement is calculated which is more precise than the first guess.
6. Repeat steps 2 to 5 until the error is small enough.

The procedure above gives the solution for displacement $\mathbf{u}$ given the external load $\mathbf{f}_{ext}$. Following this procedure for each load step the curve of the displacement can be traced. In that case one speaks of an incremental iterative procedure.

2.4 Equation of motion and eigenfrequencies

If the static equilibrium is extended to the dynamic situation one adds the inertia effects

$$\mathbf{M}\ddot{\mathbf{u}} + \mathbf{f}_{int}(\mathbf{u}) = \mathbf{f}_{ext} \tag{2.52}$$

which is an N long set of equations. $\mathbf{M}$ is the mass matrix of the structure with dimensions $[N \times N]$. The equation of motion can be linearized to

$$\mathbf{M}\ddot{\mathbf{u}} + \mathbf{K}_{tan}\mathbf{u} = \mathbf{f}_{ext} \tag{2.53}$$

In that case one can compute the eigenfrequencies by assuming

$$\mathbf{u} = \mathbf{x}e^{i\omega t} \tag{2.54}$$

$$\ddot{\mathbf{u}} = -\omega^2\mathbf{x}e^{i\omega t} \tag{2.55}$$

Substituting the DoFs $\mathbf{u}$ and their corresponding accelerations into equation 2.53 for the homogeneous case where $\mathbf{f}_{ext} = \mathbf{0}$ yields

$$\left[-\omega^2\mathbf{M} + \mathbf{K}_{tan}\right]\mathbf{x}e^{i\omega t} = \mathbf{0} \tag{2.56}$$

which must be valid for any time

$$\left[-\omega_i^2\mathbf{M} + \mathbf{K}_{tan}\right]\mathbf{x}_i = \mathbf{0} \tag{2.57}$$

This defines the eigenvalue problem that can be used to compute eigenfrequencies ω_i and eigenmodes $\mathbf{x}_i$. The eigenvalue problem describes the linearised dynamic behavior around the equilibrium position $\mathbf{u}_{eq}$ for which $\mathbf{K}_{tan}$ is evaluated.

2.5 Model order reduction in general

Reduced order modeling starts with the assumption that the displacement can be approximated as a function of a set of shapes $\mathbf{\Phi}$ times their amplitudes $\mathbf{q}$ known as generalized DoFs $\mathbf{q}$ (similar to the shape functions defined for FEM discretization)

$$\mathbf{u} = \mathbf{\Phi}\boldsymbol{q} \tag{2.58}$$

where $\mathbf{\Phi}$ is a matrix with dimension $N \times R$ where $R << N$. The number of vectors in the basis r determines the number of generalized degrees of freedom that remain after the reduction.
These shapes in the basis can be anything, but classical examples are

- Eigenmodes
- Static modes
- Second order modes
- Modes resulting from a POD analysis of a nonlinear displacement curve

Introducing the approximated displacement and their corresponding accelerations

$$\ddot{\mathbf{u}} = \mathbf{\Phi}\ddot{\boldsymbol{q}} \tag{2.59}$$

into equations of motion 2.53 one finds

$$\mathbf{M}\mathbf{\Phi}\ddot{\boldsymbol{q}} + \mathbf{f}_{int}(\mathbf{\Phi}\boldsymbol{q}) = \mathbf{f}_{ext} + \mathbf{r} \tag{2.60}$$

where $\mathbf{r}$ is the reduction error or residual made by restricting the allowable displacement to the space spanned by the chosen reduction basis $\mathbf{\Phi}$.
The next step is to restrict to allowable error to the space orthogonal to the basis which is done by projection of equation 2.60 on the reduction basis

$$\mathbf{\Phi}^T\mathbf{r} = \mathbf{0} \tag{2.61}$$

thus

$$\mathbf{\Phi}^T\mathbf{M}\mathbf{\Phi}\ddot{\boldsymbol{q}} + \mathbf{\Phi}^T\mathbf{f}_{int}(\mathbf{\Phi}\boldsymbol{q}) = \mathbf{\Phi}^T\mathbf{f}_{ext} \tag{2.62}$$

which can be written

$$\mathbf{M}_{red}\ddot{\boldsymbol{q}} + \mathbf{\Phi}^T\mathbf{f}_{int}(\mathbf{\Phi}\boldsymbol{q}) = \mathbf{f}_{red} \tag{2.63}$$

where the subscript '*red*' denotes the matrices in the reduced system. The matrix $\mathbf{f}_{red}$ with dimensions $[R \times N]$ is the modal participation of the force. Hereby the size of the equations is reduced to R with R unknowns.
In the linear case $\mathbf{f}_{int}(\mathbf{\Phi}\boldsymbol{q})$ simplifies to $\mathbf{K}_{lin}\mathbf{\Phi}\boldsymbol{q}$ therefore the reduced equation of motion simplifies to:

$$\mathbf{M}_{red}\ddot{\boldsymbol{q}} + \mathbf{\Phi}^T\mathbf{K}_{lin}\mathbf{\Phi}\boldsymbol{q} = \mathbf{f}_{red} \tag{2.64}$$

or

$$\mathbf{M}_{red}\ddot{\boldsymbol{q}} + \mathbf{K}_{red}\boldsymbol{q} = \mathbf{f}_{red} \tag{2.65}$$

Further in this report the analysis using MOR is referred to as the "reduced analysis" and the solution of the unreduced system is called the "full analysis".
If the reduction basis is filled with eigenmodes

$$\mathbf{\Phi} = [\mathbf{x}_i], \quad i = 1 \dots R \tag{2.66}$$

and the problem is nonlinear, there arises a problem. The eigenmodes are found using the linear stiffness matrix in equation 2.57 which is $\mathbf{K}_{tan}(\mathbf{u} = 0)$, thus these eigenmodes are valid as long as the system is in the linear region. When the structure undergoes large displacements, the stiffness matrix changes as it is a function of displacements, hence the eigenmodes change with displacement. Thus a reduction basis that contains only eigenmodes can not be used for nonlinear calculations as it the stiffness matrix is assumed to be constant while computing eigenmodes and thus the eigenmodes simply neglect the change in stiffness due to 'higher order terms' mentioned in equation 2.51. Because the nonlinear effects become significant mainly at larger displacements, it is likely that the modes have changed significantly when nonlinear effects become important. Therefore the reduction basis filled with only the original eigenmodes can be too restrictive, it does not allow for displacements that actually induce the proper nonlinear effects.
On the other hand it is also not possible to compute for the eigenmodes for each and every load increment as it is a very computationally expensive task. In the next section one way to overcome this problem is introduced.

2.6 Second order modes

As has just been mentioned eigenmodes in the reduction basis do not capture the change in stiffness due to change in displacement. One method to overcome this problem is to use second order modes. Second order modes give a measure of how modes change with respect to displacement.
The meaning and derivation of second order modes can be understood by starting with the tangent stiffness matrix. The tangent stiffness matrix $\mathbf{K}_{tan}$ is a function of the displacement $\mathbf{u}$ around which the linearisation has been found, $\mathbf{K}_{tan}(\mathbf{u})$.
Assume that this displacement is equal to a mode shape $\mathbf{x}_i$ times some modal amplitude α_i

$$\mathbf{u} = \mathbf{x}_i \alpha_i \tag{2.67}$$

Therefore the eigenvalue problem needed to compute another mode $\mathbf{x}_j$ is

$$\left[-\omega_j^2 \mathbf{M} + \mathbf{K}_{tan}(\alpha_i)\right] \mathbf{x}_j = 0 \tag{2.68}$$

In that case the mode $\mathbf{x}_j$ is a function of α_i. A first order approximation of how mode $\mathbf{x}_j$ changes when the displacement grows in the direction of $\mathbf{x}_i$ is given by the derivative

$$\mathbf{x}_{ji} = \frac{\partial \mathbf{x}_j}{\partial \alpha_i} \tag{2.69}$$

This sensitivity is known as the second order mode. Therefore the second order mode shows how mode j changes if the load on structure excites mode i.
To compute the sensitivity first the complete eigenvalue problem is differentiated with respect to α_i (assuming $\mathbf{M}$ constant)

$$\left(\mathbf{K}_{tan} - \omega_j^2 \mathbf{M}\right) \frac{\partial \mathbf{x}_j}{\partial \alpha_i} = \left(-\frac{\partial \mathbf{K}_{tan}}{\partial \alpha_i} + \frac{\partial \omega_j^2}{\partial \alpha_i} \mathbf{M}\right) \mathbf{x}_j \tag{2.70}$$

Which is very difficult to solve because the matrix $\left(\mathbf{K}_{tan} - \omega_j^2 \mathbf{M}\right)$ is singular. Therefore it is often simplified by neglecting mass $\mathbf{M} = \mathbf{0}$, since it has been shown that by increasing $\mathbf{M}$ by a factor γ the modes $\mathbf{x}_k$ decrease by the same factor γ, but their shapes will not change [14]

$$K_{tan} \frac{\partial \mathbf{x}_j}{\partial \alpha_i} = \left(-\frac{\partial \mathbf{K}_{tan}}{\partial \alpha_i}\right) \mathbf{x}_j \tag{2.71}$$

This can be written as [15]

$$K_{tan} \frac{\partial \mathbf{x}_j}{\partial \alpha_i} = \mathbf{g}(\mathbf{x}_i, \mathbf{x}_j) \tag{2.72}$$

Thus the second order mode follows from

$$\mathbf{x}_{ij} = \mathbf{K}_{tan}^{-1} \mathbf{g}(\mathbf{x}_i, \mathbf{x}_j) \tag{2.73}$$

under the orthogonality condition $\mathbf{x}_i \mathbf{M} \mathbf{x}_{jk} = 0$, where the pseudo load vector $\mathbf{g}$ is the sum over the elemental contributions

$$\mathbf{g}(\mathbf{x}_i, \mathbf{x}_j) = -\frac{1}{2} \sum_e A^e \left(\mathbf{n}_i^{e^T} \mathbf{C}^e(\mathbf{x}_j) + \mathbf{n}_j^{e^T} \mathbf{C}^e(\mathbf{x}_i) + \mathbf{x}_j^{e^T} \mathbf{C}_i^{e^T} \mathbf{D} B^e\right)^T \tag{2.74}$$

where $\mathbf{n}_i$ is the stress variation induced by a mode (the stress-mode)

$$\mathbf{n}_i = \mathbf{DBx}_i \tag{2.75}$$

and A^e is the area of the element.

If the second order modes are used to overcome the problem of a too restrictive reduction basis, they are included in the basis directly

$$\mathbf{\Phi} = \left[\begin{array}{cc} \mathbf{x}_i & \mathbf{x}_{ij} \end{array} \right], \quad i = 1 \ldots R, \quad j = 1 \ldots R \tag{2.76}$$

2.7 Verification of the JW by Ansys

The finite element discretisation along with the mathematical model (full model) is programmed in Matlab for the JW. The structure is also simulated in Ansys, which is a commercial FE analysis tool and sets up the mathematical model internally. Figure 2.4 shows the geometry of the JW. The material used is aluminum with density $\rho = 2.7 \times 10^{-6} Kg/mm^3$, Young's modulus of $E = 69GPa$ and Poisson ratio $\nu = 0.33$. The thickness of the plates is $2mm$ except for the slope plate which has a thickness of $0.5mm$. The structure is clamped at lines shown with 'C' in the figure. The structure is subjected to a uniform vertical (in $-z$ direction) pressure of $P = 0.55125 Kg/(mm.s^2)$ corresponding to a dynamic pressure of a speed of $v = 30m/s$ [5].

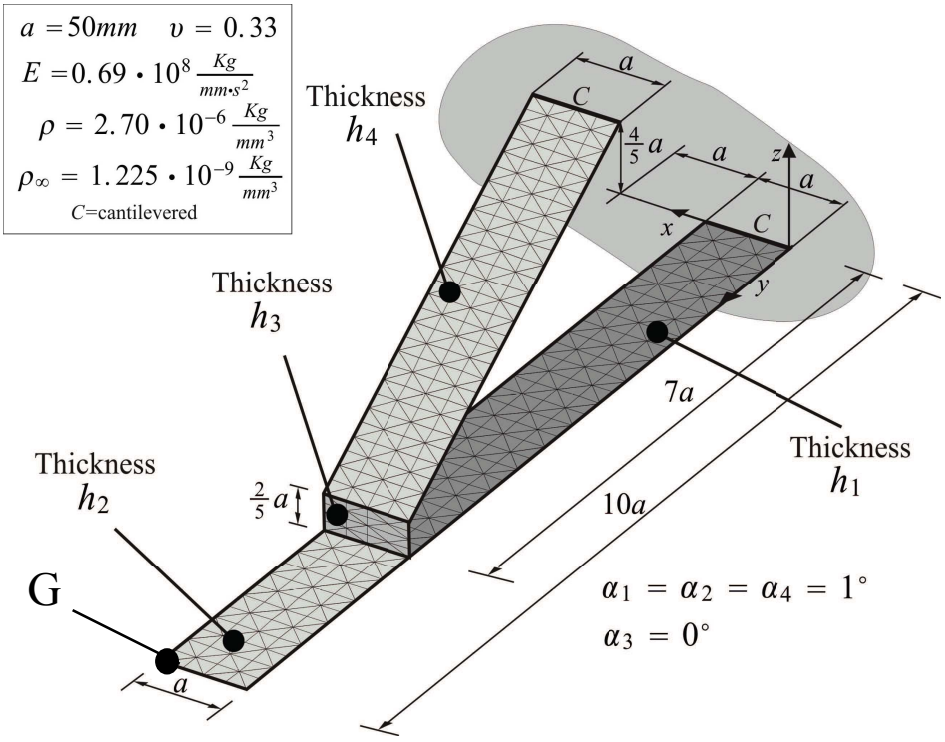

Figure 2.4: Joined Wing model geometry and material properties. $h_1 = h_2 = h_3 = 2mm$ and $h_4 = 0.5mm$ [5].

The response obtained by Matlab is compared with response obtained by Ansys for the node at $[50, 500, 0]$, which is shown with letter G in figure 2.4. Figures 2.5,

2.6 and 2.7 show the comparison between Matlab and Ansys for the displacement of this node in x, y and z direction respectively. There is a good match between the two results. In figure 2.5 the curves are not exactly the same but it should be noticed that the displacement in the x direction is very small (in the order of $10^{-3}mm$) because the pressure is applied in the vertical direction z. These results suggest that the simplified kinematic equations sufficiently agree with the more advanced kinematic equations in Ansys and that the Matlab model suffices for the investigation in this thesis.

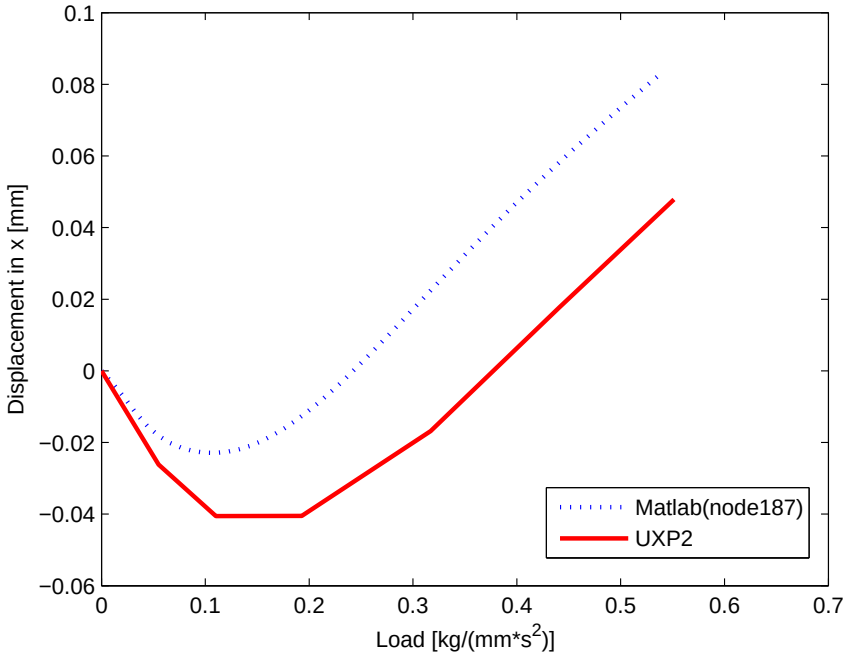

Figure 2.5: Comparison between Matlab and Ansys for displacement of the node with coordinates $[50, 500, 0]$ in x direction.

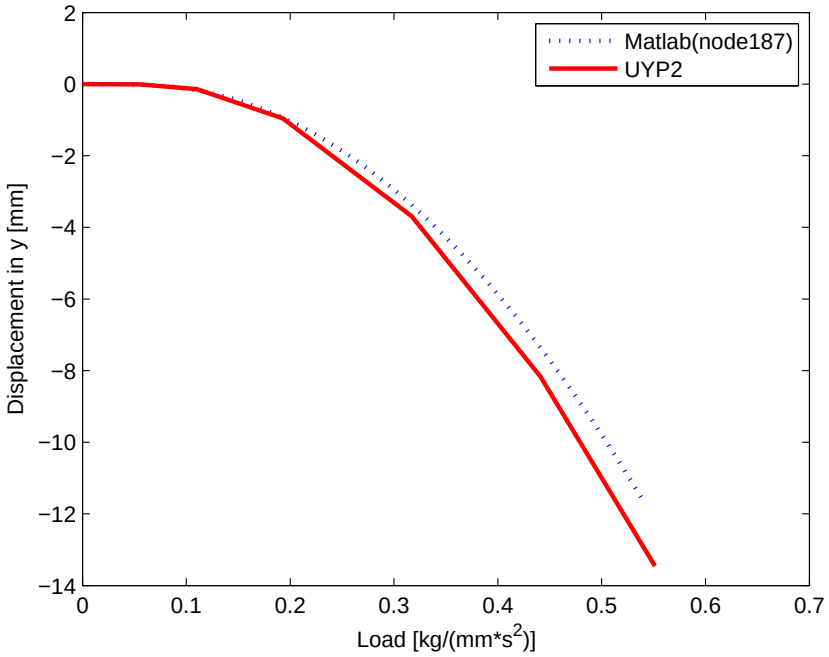

Figure 2.6: Comparison between Matlab and Ansys for displacement of the node with coordinates $[50, 500, 0]$ in y direction.

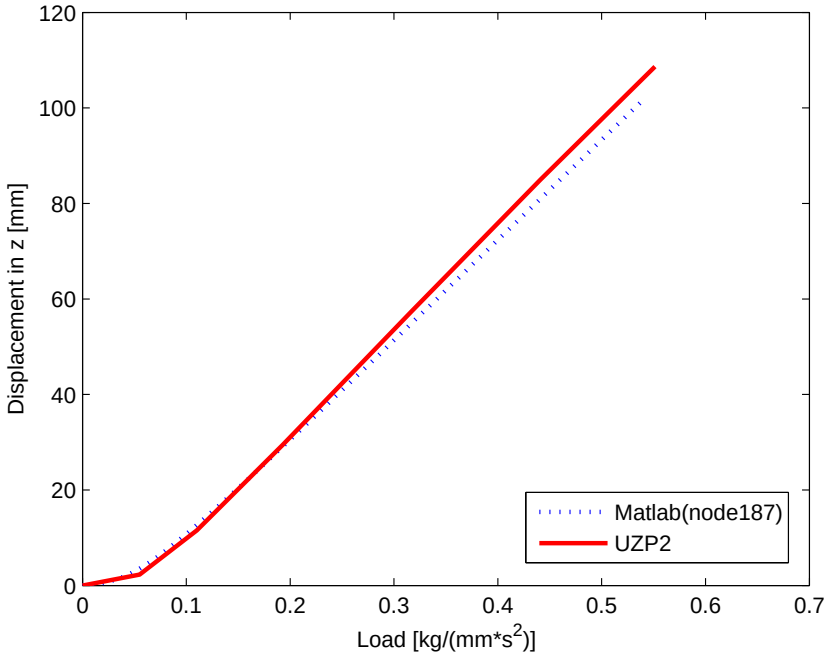

Figure 2.7: Comparison between Matlab and Ansys for displacement of the node with coordinates $[50, 500, 0]$ in z direction.

Chapter 3

Literature Review

3.1 Optimal second order reduction basis selection for nonlinear transient analysis

This section summarises [16]. For geometrically nonlinear structural dynamics problems, the model is reduced by projecting the finite element (FE) equations on a basis containing vibration mode (VM) and associated modal derivative (MD). The dimension of this basis however can become very large considering that the number of MDs are quadratic with respect to the number of chosen VMs. Considering the fact that large displacements may occur in aeronautics and that minimum weight is a design factor, it is important to consider nonlinearity. Therefore effective model order reduction is necessary. In order to reduce the number of DoF, several VMs of the structure at a certain dynamic equilibrium are extracted and form a reduction basis. Then the dynamic equations are projected on the basis. Although this is a common approach to reduce DoFs, high frequency VMs can be very important for nonlinear systems, these modes are expensive to calculate for a large FE model. A major issue in nonlinear structural applications is the bending-stretching coupling, arising from the finite out of plane displacements a slender or thin-walled structure exhibits during operation. Typically, low frequency VMs are bending dominated and do not contain the proper membrane displacement contribution which is necessary to accurately represent the effect of the nonlinearity [16]. Including higher order modes in the reduction basis can enrich the basis and no expensive computing is needed. Higher order modes or MDs are the derivative of the linear eigenmodes with respect to the modal amplitudes. Because the number of MDs is quadratic with respect to the chosen VMs, these VMs and MDs should be selected effectively.
The discretized, N dimensional, nonlinear, undamped FE equations of motions are as follows

$$\mathbf{M}\ddot{\mathbf{u}} + \mathbf{f}_{int}(\mathbf{u}) = \mathbf{f}(t) \tag{3.1}$$

where $\mathbf{u}$ is the generalized displacement vector, $\mathbf{M}$ is the mass matrix, $\mathbf{f}_{int}(\mathbf{u})$ is the nonlinear force vector and $\mathbf{f}(t)$ is the applied force. The initial conditions are zero. The nonlinearity of $\mathbf{g}(\mathbf{u})$ is caused by geometrical effects only, that is when the displacements are so large that a linear kinematic model does not hold, the thin-walled structure stays in the elastic range. In order to reduce the number of DoFs, we approximate the displacement $\mathbf{u}$

$$\mathbf{u}_{N\times 1} = \mathbf{\Phi}_{N\times R}\mathbf{q}(t) \tag{3.2}$$

where $\mathbf{\Phi}$ is a suitable reduction basis and $R << N$. Projecting equation 3.1 on this basis results in

$$\mathbf{\Phi}^T\mathbf{M}\mathbf{\Phi}\ddot{\mathbf{q}}(t) + \mathbf{\Phi}^T\mathbf{f}_{int}(\mathbf{\Phi}\mathbf{q}) = \mathbf{\Phi}^T\mathbf{f}(t) \tag{3.3}$$

$$\hat{\mathbf{M}}\ddot{\mathbf{q}}(t) + \hat{\mathbf{f}_{int}}(\mathbf{\Phi}\mathbf{q}) = \hat{\mathbf{f}} \tag{3.4}$$

The solution of equation 3.1 is referred to as the full solution and the solution to equation 3.4 is referred to as the reduced solution. The reduction basis $\mathbf{\Phi}$ in this case is formed by VMs ($\mathbf{x}_i$) and MDs ($\mathbf{x}_{ij}$), therefore $\mathbf{\Phi} = [\ \mathbf{x}_i \quad \mathbf{x}_{ij}]$. The VMs are calculated using the linear equation of motion around an equilibrium. The MDs are defined as follows (see also the previous chapter)

$$\mathbf{x}_{ij} = \frac{\partial \mathbf{x}_i}{\partial \mathbf{q}_j} \tag{3.5}$$

where $\mathbf{x}_i$ are the calculated VMs and $\mathbf{q}_j$ are the associated modal amplitudes. This equation shows how a certain mode $\mathbf{x}_i$ changes if the structure is displaced according to the shape described by mode $\mathbf{x}_j$.
The big advantage of this method is that the most important contributions can be estimated prior the actual calculation of the MDs, here follows how. By calculating of R, VMs and their associated eigenfrequencies ω_i, we can approximate the response $\mathbf{u}(t)$

$$\mathbf{u}(t) = \sum_{i=1}^{M} \frac{\mathbf{x}_i\mathbf{x}_i^T\mathbf{f}}{\mu_i} \int_0^t \frac{\sin(\omega_i(t-\tau))}{\omega_i}\phi(\tau)d\tau = \sum_{i=1}^{k} \alpha_i\theta_i(t) \tag{3.6}$$

here $\mu_i = \Phi_i^T\mathbf{M}\Phi_i$ is the modal mass associated to the mode number i. The convergence of this approximation depends on a quasi-static contribution (associated to the spatial factors α_i) and a spectral contribution, which is determined by the convergence of the convolution integral in equation 3.6.

$$\alpha_i = \frac{\mathbf{x}_i\mathbf{x}_i^T\mathbf{f}}{\mu_i} \tag{3.7}$$

implies that the load shape $\mathbf{f}$ has to be nearly orthogonal to the $N - R$ modes left out of the approximation. The temporal factors $\theta_i(t)$ depend in general on the frequency content of the system and of the applied load. We consider two cases:

- for a step load $\phi(t) = 1$ for $t > 0$

$$\theta_i(t) = \frac{1 - \cos(\omega_i t)}{\omega_i^2} \tag{3.8}$$

- for a harmonic load $\phi(t) = \cos(\Omega t)$

$$\theta_i(t) = \frac{\omega_i \sin(\Omega t) - \Omega \sin(\omega_i t)}{\omega_i(\omega_i^2 - \Omega^2)} \tag{3.9}$$

We can now assume that the R VMs will interact when nonlinearity is considered. Another assumption is that the contribution of the MDs is of second order and their mutual relevance could be indicated by:

- for step load

$$b^{ij}_{step} = \frac{|\alpha_i||\alpha_j|}{\omega_i^2 \omega_j^2} \tag{3.10}$$

- for harmonic load

$$b^{ij}_{harm} = |\alpha_i||\alpha_j|\beta_i\beta_j \qquad \beta_k(\Omega) = |\frac{1}{\omega_k^2 - \Omega^2}| + |\frac{\Omega}{\omega_k(\omega_k^2 - \Omega^2)}| \tag{3.11}$$

The factors b^{ij}_{step} and b^{ij}_{harm} indicate the relative amplitude of the MD mode $\mathbf{x}_{ij}$ given the contribution of $\mathbf{x}_i$ and $\mathbf{x}_j$ to the linear solution. The most relevant MDs will be the ones with the highest values of the corresponding b^{ij} coefficients.
These methods are used further in a numerical example for a simple cantilever. It shows that by using the most relevant MDs in the reduction basis, the dynamic response of the loaded cantilever in the reduced solution agrees with the full solution.
The power of this method lies in the second order modes enrichment can be seen as higher order expansion of the solution. Therefore the convergence properties of the base linearized problem should naturally provide a guideline also for the higher order expansion.

This paper forms the basis of the research that is done in this report. The modal derivatives are a powerful ... to compensate for the high frequency vibration modes. The question that arises however, is that why this method fails to give accurate results for the JW.

3.2 A reduced order nonlinear aeroelastic analysis of joined wings based on the proper orthogonal decomposition

This section summarises [5]. In this paper, a method is introduced in order to reduce the order of the nonlinear analysis for the JW. Here the method of snapshots is used which is an efficient method when the resolution of the domain in space (N) is higher than the number of observations. The method of snapshots which can be used both for numerical and / or experimental observations is based on the fact that the data vectors (snapshots $\mathbf{u}_i$), and the eigenvectors $\mathbf{x}_k$ span the same linear space. At each load step, the solution is calculated and these solutions form the snapshots. Furthermore the Proper Orthogonal Decomposition (POD) method is used which is based on Singular Value Decomposition (SVD), a useful factorization method which gives the eigenvectors and eigenvalues of a matrix multiplied by its transpose.

First the eigenvectors of the linear equations of motion around an equilibrium point are calculated and a reduction basis is formed with the first low frequency eigenvectors. Then the snapshots which are displacement vectors from increasing load steps are calculated. At each snapshot, the tangent stiffness matrix is calculated. Using this tangent stiffness matrix, we can have new set of eigenmodes. POD is used to factorize the matrix of eigenmodes and in each snapshot this POD is updated. This gives a nonlinear description of the eigenmodes in POD modes as a function of the load. These eigenmodes are used as reduction basis. Therefore the basis is updated at each time step.

The procedure of updating the structural tangent modes for each load step, results in excellent approximation of the full order solution for a joined wing and a delta wing if this approach used to interpolate. The use of the POD modes to extrapolate the results, shows that the extrapolation is only accurate if the the aerodynamic speed is increase for about 10%. Therefore it is impossible to really extrapolate using this method, only interpolation gives really accurate results.

3.3 Model reduction tools for nonlinear structural dynamics

This section summarises [14]. Despite the increase of computer capacities, reduction techniques for FE systems are still very interesting. An important factor for the reduction technique to be successful lies in the selection of the basic vectors (modes of the structure at a certain time instant with a certain deformation). Proper selection of basic vectors results in maximum result quality and minimum effort of the computation time for the reduced system integration and minimum effort to obtain these modes.
Using momentum equations, strain relations with initial and boundary conditions, the system of N nonlinear equations for a finite element model is obtained

$$\mathbf{M}\ddot{\mathbf{u}}(t) = \mathbf{f}_{ext}(t) - \mathbf{f}_{int}(\mathbf{u}(t)) \qquad with \qquad \mathbf{u}(t=0) = \mathbf{u}_0 \qquad \dot{\mathbf{u}}(t=0) = \mathbf{v}_0 \tag{3.12}$$

where $\mathbf{M}$ is the mass matrix, $\mathbf{u}(t)$ is a column matrix containing the nodal DoFs, $\mathbf{f}_{int}(\mathbf{u}(t))$ is the internal nodal forces and $\mathbf{f}_{ext}(t)$ is the external nodal forces. We consider systems without damping. In this paper only geometrical nonlinearities are considered but the derivations still hold when applying material nonlinearities.
We reduce the system of N equation (N unknowns) by approximating the nodal DoFs

$$\mathbf{u}(t) = \mathbf{u}_0 + \mathbf{\Phi}\mathbf{q}(t) \tag{3.13}$$

where $\mathbf{\Phi}$ is the reduction matrix of size $N \times R$ ($R << N$) and $\mathbf{q}(t)$ the modal coordinates are the set of R new unknowns which are easier to compute as R is much smaller than N. Vector $\mathbf{u}_0$ denotes the initial displacements of the structure; also the columns of the reduction matrix (modes of the structure) are calculated using this initial state. Substituting equation 3.13 in equation 3.12 and premultiplying by the transpose of the reduction matrix results in the reduced nonlinear system

$$\mathbf{M}_{red}\ddot{\mathbf{q}}(t) + \mathbf{\Phi}^T\mathbf{f}_{int}(\mathbf{u}_0 + \mathbf{\Phi}\mathbf{q}) = \mathbf{f}_{red}(t) \tag{3.14}$$

$$\mathbf{M}_{red} = \mathbf{\Phi}^T\mathbf{M}\mathbf{\Phi}, \qquad \bar{\mathbf{f}}_{red} = \mathbf{\Psi}^T\mathbf{f}_{ext} \tag{3.15}$$

The modes used in the reduction basis can be tangent modes which are eigenvectors obtained by solving the eigenvalue problem, linearized around an initial configuration. Consider the FE system in an initial state with nodal displacements $\mathbf{u}_0$. The system is linearized around $\mathbf{u}_0$, using the tangent stiffness matrix

$$\mathbf{K}_{tan}(\mathbf{u} = \mathbf{u}_0) = \frac{\partial \mathbf{f}_{int}}{\partial \mathbf{u}}(\mathbf{u} = \mathbf{u}_0) = \mathbf{K}_{lin} \tag{3.16}$$

Tangent modes are then determined from the eigenvalue problem

$$(\mathbf{K}_{tan} - \omega_p^2\mathbf{M})\mathbf{x}_p = 0 \qquad p = 1 \ldots N \tag{3.17}$$

From now on in this section $\mathbf{K}_{tan}$ will be written simply as $\mathbf{K}$. If the reduction basis has the first p tangent modes, then we have a linear approximation of nodal DoFs (equation 3.13) in the ordinary modal coordinates α_p which is a good approximation only around $\mathbf{u}_0$. Reduced coordinates $\mathbf{q}$ are then the same as α_p and equation 3.13 becomes

$$\mathbf{u} - \mathbf{u}_0 = \sum_{p=1}^{R} (\mathbf{x}_p \alpha_p) = \mathbf{\Phi q} \tag{3.18}$$

If the system is nonlinear, these modes change for large deformations and therefore fail to describe the system. Adding second order terms consisting of modal derivatives to the reduction basis can improve the description of the system.
For large deformations the tangent stiffness matrix changes a lot. As a result the tangent modes also change, as a function of $\mathbf{u}$ and α_p. So with all N tangent modes equation 3.18 can be written as

$$\mathbf{u} - \mathbf{u}_0 \equiv \Delta\mathbf{u} = \sum_{p=1}^{N} (\mathbf{x}_p(\mathbf{u}) \alpha_p) = \mathbf{\Phi q} \tag{3.19}$$

Assume $\Delta\mathbf{u}$ can be evaluated around its starting configuration $\Delta\mathbf{u} = 0$ by a second order Taylor series

$$\Delta\mathbf{u} = \sum_{p=1}^{N} \left(\frac{\partial \Delta\mathbf{u}}{\partial \alpha_p}(\alpha = 0)\alpha_p + \sum_{r=1}^{r} \left(\frac{\partial^2 \Delta\mathbf{u}}{\partial \alpha_p \partial \alpha_r}(\alpha = 0)\frac{\alpha_r}{2} \right) \alpha_p \right) \tag{3.20}$$

where the derivatives of the nodal displacements are calculated using equation 3.19

$$\frac{\partial \Delta\mathbf{u}}{\partial \alpha_p} = \mathbf{x}_p + \sum_{p=1}^{N} \left(\frac{\partial \mathbf{x}_r}{\partial \alpha_p} \alpha_r \right) \tag{3.21}$$

$$\frac{\partial^2 \Delta\mathbf{u}}{\partial \alpha_p \partial \alpha_r} = \frac{\partial \mathbf{x}_r}{\partial \alpha_p} + \frac{\partial \phi_p}{\partial \alpha_r} + \sum_{l=1}^{N} \left(\frac{\partial^2 \mathbf{x}_l}{\partial \alpha_p \alpha_r} \alpha_l \right) \tag{3.22}$$

At $\mathbf{u}_0$ the ordinary modal coordinates α are zero. The nodal displacement derivatives of equation 3.22 become

$$\frac{\partial \Delta\mathbf{u}}{\partial \alpha_p}(\alpha = 0) = \mathbf{x}_p(\mathbf{u} = \mathbf{u}_0) \tag{3.23}$$

$$\frac{\partial^2 \Delta\mathbf{u}}{\partial \alpha_p \partial \alpha_r}(\alpha = 0) = \frac{\partial \mathbf{x}_r}{\partial \alpha_p}(\mathbf{u} = \mathbf{u}_0) + \frac{\partial \mathbf{x}_p}{\partial \alpha_r}(\mathbf{u} = \mathbf{u}_0) \tag{3.24}$$

In the presence of nonlinearities the reduction matrix can be made of p ordinary tangent modes and $R - p$ derivatives as in second part of equation 3.24. Then $\mathbf{q}$ contains p ordinary modal coordinates α_p and $R-p$ kind of quadratic ordinary modal coordinates. Three ways for calculating modal derivatives $\partial \mathbf{x}_r / \partial \alpha_p$ are studied.

1. Analytical approach using mass consideration: To find a modal derivative, $\partial \mathbf{x}_r / \partial \alpha_p$, we differentiate the eigenvalue problem equation 3.17

$$(\mathbf{K} - \omega_r^2 \mathbf{M}) \frac{\partial \mathbf{x}_r}{\partial \alpha_p} = \left(\frac{\partial \omega_r^2}{\partial \alpha_p} \mathbf{M} - \frac{\partial \mathbf{K}}{\partial \alpha_p} \right) \mathbf{x}_r \tag{3.25}$$

where the derivation of the tangent stiffness matrix is done numerically as follows

$$\frac{\partial \mathbf{K}}{\partial \alpha_p} \approx \frac{\mathbf{K}(\mathbf{u}_0 + \mathbf{x}_p \delta\alpha_p) - \mathbf{K}(\mathbf{u}_0)}{\delta\alpha_p} \tag{3.26}$$

If two tangent modes (ϕ_r and ϕ_{r+1}) belong to the same ω_r, then the matrix $(\mathbf{K} - \omega_r^2\mathbf{M})$ is not full rank $(N-2)$ and these tangent modes are the null space of this matrix. The general solution of $\partial\phi_r/\partial\alpha_p$ is the sum of the homogeneous and particular solutions. The homogeneous solution is equal to

$$\left\{\frac{\partial \mathbf{x}_r}{\partial \alpha_p}\right\}_{hom} = \sum_{i=1}^{2} \beta_i \mathbf{x}_{r+i-1} \tag{3.27}$$

To find the particular solution, the right hand side of equation 3.25 must satisfy two conditions. To find these conditions we first represent the unknown particular solution in a new basis by using a transformation matrix $\mathbf{T}$

$$\left\{\frac{\partial \mathbf{x}_r}{\partial \alpha_p}\right\}_{par} = \mathbf{T}\left\{\frac{\partial \mathbf{x}_r}{\partial \alpha_p}\right\}' \tag{3.28}$$

Matrix $\mathbf{T}$ is the unity matrix except that its k^{th} and l^{th} column are the tangent modes ϕ_r and ϕ_{r+1} respectively. Numbers k and l are chosen in a way that $\mathbf{T}$ would not be singular. Substituting 3.28 in equation 3.25 and premultiplying by $\mathbf{T}^T$ we get

$$\mathbf{T}^T(\mathbf{K} - \omega_r^2\mathbf{M})\mathbf{T}\left\{\frac{\partial \mathbf{x}_r}{\partial \alpha_p}\right\}' = \mathbf{T}^T\left(\frac{\partial \omega_r^2}{\partial \alpha_p}\mathbf{M} - \frac{\partial \mathbf{K}}{\partial \alpha_p}\right)\mathbf{x}_r \tag{3.29}$$

where the k^{th} and l^{th} equations are as follows

$$0 = \mathbf{x}_r^T \mathbf{M}\mathbf{x}_r \frac{\partial \omega_r^2}{\partial \alpha_p} - \mathbf{x}_r^T \frac{\partial \mathbf{K}}{\partial \alpha_p}\mathbf{x}_r \tag{3.30}$$

$$0 = \mathbf{x}_{r+1}^T \mathbf{M}\mathbf{x}_r \frac{\partial \omega_r^2}{\partial \alpha_p} - \mathbf{x}_{r+1}^T \frac{\partial \mathbf{K}}{\partial \alpha_p}\mathbf{x}_r \tag{3.31}$$

which when normalized with respect to the mass matrix, are

$$\frac{\partial \omega_r^2}{\partial \alpha_p} = \mathbf{x}_r^T \frac{\partial \mathbf{K}}{\partial \alpha_p}\mathbf{x}_r \tag{3.32}$$

$$0 = \mathbf{x}_{r+1}^T \frac{\partial \mathbf{K}}{\partial \alpha_p}\mathbf{x}_r \tag{3.33}$$

Because the k^{th} and l^{th} columns and rows of $\mathbf{T}^T(\mathbf{K} - \omega_r^2\mathbf{M})\mathbf{T}$ are full of zeros the k^{th} and l^{th} equation of equation 3.29 can be left out. Subsequent substitution of equation 3.32 into equation 3.29 gives the final equation which can be solved to give the modal derivative, without the k^{th} and l^{th} entries. These entries should be zero. Thereafter the result is transformed using equation 3.28 to give the particular solution.

2. Analytical approach excluding mass consideration The mass of the system does not have any effect on the shape of the modal derivatives, as a decrease γ in the modal derivatives can be shown by multiplying the mass matrix by γ. Now we can simplify equation 3.25 by neglecting the inertia terms

$$\frac{\partial \mathbf{x}_r}{\partial \alpha_p} = -\mathbf{K}^{-1}\frac{\partial \mathbf{K}}{\partial \alpha_p}\mathbf{x}_r \tag{3.34}$$

and rigid body modes are prevented. Because of the symmetry of the modal derivatives

$$\frac{\partial \mathbf{x}_r}{\partial \alpha_p} = \frac{\partial \mathbf{x}_p}{\partial \alpha_r} \tag{3.35}$$

the number of modal derivative evaluations using this method is less than the previous and the next methods.

3. Numerical approach to determine modal derivatives In this method the modal derivative is found by varying the p^{th} ordinary modal coordinate and its influence on the tangent stiffness matrix is computed by calculating $\mathbf{K}(\mathbf{u}_0)$ and $\mathbf{K}(\mathbf{u}_0 + \mathbf{x}_p\delta\alpha_p$. Using these two stiffness matrices, two eigenvalue problems are solved and the modal derivative is found as follows

$$\frac{\partial \mathbf{x}_r}{\partial \alpha_p} \approx \frac{\mathbf{x}_r(\mathbf{u}_0 + \mathbf{x}_p\delta\alpha_p) - \mathbf{x}_r(\mathbf{u}_0)}{\delta\alpha_p} \tag{3.36}$$

Now we consider the application of static modes to the reduction process. 'Static modes are the steady state solution to the originally nonlinear dynamic system and they depend on the external loads applied to the system. Static modes are obtained by an incremental Newton-Raphson iteration procedure, where inertia terms are not considered'. Hereby the nonlinear set of algebraic equations is

$$\mathbf{f}_{ext} - \mathbf{f}_{int}(\mathbf{u}) = \mathbf{0} \tag{3.37}$$

Furthermore the combinations of modes and modal derivatives obtained by these methods, is used to solve two FE problems with 13 and 39 DoFs and the results are compared.
Using analytical approach including mass consideration, good results are obtained which are in agreement with the results obtained by using numerical approach. Results from the reduction matrices containing only tangent modes are not acceptable, modal derivatives should be added to the reduction basis to improve the reduced solutions. Hereby the addition of static modes to the reduction basis (with tangent modes and modal derivatives) can give better solutions but these are not generalisable.

3.4 Rigorous improvement of semi-analytical design sensitivities by exact differentiation of rigid body motions

This section summarises [17]. Computing shape design sensitivities using the semi-analytical method show inaccuracy problems which are due to the numerical differentiation of the finite element stiffness matrices. These inaccuracies become specially

dominant when the individual elements have large rigid body motions. In this paper a method is introduced to overcome these inaccuracies by exact differentiation of the rigid body motions. Static analysis of a linear mechanical structure lead to the governing equations

$$\mathbf{K}(\mathbf{d})\mathbf{u}(\mathbf{d}) = \mathbf{f}(\mathbf{d}) \tag{3.38}$$

where $\mathbf{K}(\mathbf{d})$ is the symmetric stiffness matrix, $\mathbf{u}(\mathbf{d})$ is the vector of nodal displacements and $\mathbf{f}(\mathbf{d})$ is the vector of external loads. Here $\mathbf{d}$ denotes the set of design variables that the sensitivities are taken with respect to them. Differentiating this equation w.r.t. the design variables gives

$$\mathbf{K}'\mathbf{u} + \mathbf{K}\mathbf{u}' = \mathbf{f}' \tag{3.39}$$

$$\mathbf{u}' = \mathbf{K}^{-1}(\mathbf{f}' - \mathbf{K}'\mathbf{u}) \tag{3.40}$$

where the term $\mathbf{q} = \mathbf{f}' - \mathbf{K}'\mathbf{u}$ is referred to as the pseudo load vector. In this method the nodal displacement vector for each element ($\mathbf{u}_e$) is decomposed into a part containing pure deformations and a part containing rigid body modes contributions.

$$\mathbf{u}_e = \mathbf{u}_e^\epsilon + \sum_{k=1}^{s} \frac{\mathbf{u}_e.\mathbf{r}_k}{\mathbf{r}_k.\mathbf{r}_k}\mathbf{r}_k = \mathbf{u}_e^\epsilon + \alpha^k\mathbf{r}_k \tag{3.41}$$

where $\mathbf{r}_k \qquad k = 1 \dots s$ shows the rigid body motions and $\alpha^k = (\mathbf{u}_e.\mathbf{r}_k)/(\mathbf{r}_k.\mathbf{r}_k)$. The second term in the right hand side is a projection of the displacement vector on the rigid body modes and denotes the part of $\mathbf{u}_e$ that contains rigid body mode. The pseudo load vector for a single element then reads

$$\mathbf{q}_e = \mathbf{f}'_e - \mathbf{K}'_e\mathbf{u}_e^\epsilon - \mathbf{K}'_e(\alpha^k\mathbf{r}_k) \tag{3.42}$$

where the last term of the right hand side can be written as

$$\mathbf{K}'_e(\alpha^k\mathbf{r}_k) = \alpha^k(\mathbf{K}'_e\mathbf{r}_k) = -\alpha^k(\mathbf{K}_e\mathbf{r}'_k) \tag{3.43}$$

which comes from the definition of rigid body modes and that they cause no deformations ($\mathbf{K}_e\mathbf{r} = 0$ so the differentiation w.r.t. design variables gives $\mathbf{K}'_e\mathbf{r}_k + \mathbf{K}_e\mathbf{r}'_k = 0$). The pseudo load vector now takes the form

$$\mathbf{q}_e = \mathbf{f}'_e - \mathbf{K}'_e\mathbf{u}_e^\epsilon + \alpha^k\mathbf{K}_e\mathbf{r}'_k \tag{3.44}$$

As the rigid body modes and the external load vector are function of design variables, the first and last term in the right hand side of equation 3.44 can be evaluated exactly and with minor programming effort. The middle term however is where inaccuracies come from. The errors due to approximating $\mathbf{K}'_e$ manifest themselves only in this term. However, the components of this term along the rigid body modes $\mathbf{r}_k$ can be evaluated exactly

$$\frac{\mathbf{r}_k\mathbf{K}'_e\mathbf{u}_e^\epsilon}{\mathbf{r}_k.\mathbf{r}_k} = -\frac{\mathbf{r}'_k\mathbf{K}_e\mathbf{u}_e^\epsilon}{\mathbf{r}_k.\mathbf{r}_k} \tag{3.45}$$

by using the definition of rigid body modes. Using these results the pseudo load vector is

$$\mathbf{q}_e = \mathbf{f}'_e - \mathbf{K}'_e\mathbf{u}_e^\epsilon + \left[\frac{\mathbf{r}_k\mathbf{K}'_e\mathbf{u}_e^\epsilon}{\mathbf{r}_k.\mathbf{r}_k}\right]\mathbf{r}_k + \left[\frac{\mathbf{r}'_k\mathbf{K}_e\mathbf{u}_e^\epsilon}{\mathbf{r}_k.\mathbf{r}_k}\right]\mathbf{r}_k + \alpha^k\mathbf{K}_e\mathbf{r}'_k \tag{3.46}$$

'The third term in the right hand side removes the part of contribution due to $\mathbf{K}'_e\mathbf{u}^\epsilon_e$ which is in the space spanned by $\mathbf{r}_k$. This term maybe inaccurate as $\mathbf{K}'_e$ is obtained by applying finite differences. The forth term compensates for these inaccuracies, for it is evaluated exactly. It is stressed that $\mathbf{r}'_k$ can be evaluated in an exact manner, whereas $\mathbf{K}'_e$ and $\mathbf{f}'_e$ are generally determined by their forward finite difference approximations. Thus the last two terms of equation 3.46 are computed exactly. In cases of relatively large rigid body motions, these terms may become large as compared to $\mathbf{K}'_e\mathbf{u}^\epsilon_e$. Therefore, the proposed method will drastically reduce the abnormal errors which occur in the standard sensitivity analysis method [17].'

Furthermore this paper shows how the method can be implemented for a curved triangular shell element. Furthermore this paper compares the results of traditional and refined (the method introduced) sensitivity analysis (using forward and central finite differences) with each other. The examples of a strip in tension, square plate, cantilever beam, cylindrical panel (with pure bending) and cylindrical support are used to compare different methods. Finally it can be concluded that there are three advantages of the proposed method. Firstly this method eliminates the abnormal errors due to large rigid body motions, which happened in the traditional sensitivity analysis methods. Secondly, by implementing some basic vector manipulations and defining a set of rigid body modes for each class of elements, the refined sensitivity analysis method can be easily implemented in the existing software. Thirdly, because the vector manipulations per element are not a lot, the additional computational effort is very small.

The method advocated in this paper does not promise to provide an improvement for the JW problem, because the pseudo load vector of the geometric nonlinear model is not obtained by a semi-analytic method but by a full analytic differentiation.

3.5 Asymptotic study of the elastic postbuckling behavior of structures by the finite element method

This section presents a summary of [3]. In the paper the goal is to find the nonlinear quasi-static load displacement curve during buckling. The approach is to use model order reduction. The paper starts by defining the deformation energy

$$E(\mathbf{u}) = \frac{1}{2}\mathbf{u}^T\mathbf{K}_{lin}\mathbf{u} + Q(\mathbf{u}) - \lambda\mathbf{f}^T_{ext}\mathbf{u} \tag{3.47}$$

where $\mathbf{K}_{lin}$ is the linear stiffness matrix, Q the non linear term in the deformation energy and $\lambda\mathbf{f}_{ext}$ the external load.

The linear static solution to a load $\mathbf{f}_{ext}$ is determined

$$\mathbf{u}_0 = \mathbf{K}^{-1}_{lin}\mathbf{f}_{ext} \tag{3.48}$$

Furthermore the linear buckling loads λ_i and buckling modes $\mathbf{x}_i$ are determined

$$[\mathbf{K}_{lin} - \lambda_i\mathbf{K}_G]\,\mathbf{x}_i = \mathbf{0} \tag{3.49}$$

where $\mathbf{K}_G$ is the geometric stiffness matrix.

It is subsequently assumed that the displacement at load $\lambda\mathbf{f}_{ext}$ can be written as

$$\mathbf{u} = \lambda\mathbf{u}_0 + \Sigma_{i=1\ldots r}(a_i\mathbf{x}_i) + \boldsymbol{\phi} \tag{3.50}$$

where a_i are the generalized DoFs and $\boldsymbol{\phi}$ is a correction for the data missing in the modal basis.

An approximation for $\boldsymbol{\phi}$ is computed based on substitution of (3.50) into the deformation energy, then determine the Taylor expansion of E around $\boldsymbol{\phi}$ and neglecting cubic and higer terms.

$$E(\mathbf{u}, \lambda) = P_0 + P_1(\boldsymbol{\phi}) + P_2(\boldsymbol{\phi}) + \text{neglected higher order terms} \tag{3.51}$$

where P_0 is not depending on $\boldsymbol{\phi}$, P_1 is linear in $\boldsymbol{\phi}$ and P_2 is quadratic in $\boldsymbol{\phi}$. It can be shown that

$$P_1 = \boldsymbol{\phi}^T \mathbf{g}(\lambda, a_i) \tag{3.52}$$

$$P_2 = \tfrac{1}{2}\boldsymbol{\phi}^T \mathbf{K}\boldsymbol{\phi} + \tfrac{1}{2}\boldsymbol{\phi}^T \mathbf{K}\boldsymbol{\phi} \tag{3.53}$$

where $\mathbf{K}$ is the tangent stiffness matrix, $\mathbf{C}$ is a matrix with terms that will be neglected as well and $\mathbf{g}$ is a vector depending on the load and displacement.

This energy must remain stationary to define an equilibrium, which allows the combination of the derivatives of P_i with $\boldsymbol{\phi}$ to form the equation which can be used to compute an approximation of the correction

$$\mathbf{K}\boldsymbol{\phi} = -\mathbf{g} \tag{3.54}$$

where $\mathbf{G}$ acts as a pseudo load.

It can be shown that the extra displacements required to reach the correction can be computed using:

$$\frac{\partial^2 E}{\partial a_i \partial a_j}\Delta a_j = -\frac{\partial}{2\partial a_i}(\boldsymbol{\phi}^T \mathbf{C}\boldsymbol{\phi}) \tag{3.55}$$

and the error therefore can be computed as

$$e_j = \frac{\Delta a_j}{a_j} \tag{3.56}$$

During the solution of the load displacement curve using an incremental iterative procedure the correction $\boldsymbol{\phi}$ is computed for each increment. If an error e_j is too large the correction $\boldsymbol{\phi}$ is normalized and added to the reduction basis and a correction $\boldsymbol{\phi}_{new}$ with this enhanced basis is computed. This is repeated until e_j is small enough. Therefore this approach acts as a greedy algorithm.

Chapter 4

Model Order Reduction applied to the JW Problem

The system of JW is reduced using VMs and MDs as explained in section 2.5. But because of high geometrical nonlinearities that exist in the system, this reduction basis is still not rich enough to support for the nonlinearities of the system. In this chapter we take a close look to the JW, and try to find and compensate for the missing information. Other examples that a reduction basis with VMs and MDs contain enough information are analysed. Afterwards the reason that this basis is not working for JW is further explained. Finally other methods are discussed to enrich the reduction basis.

4.1 Full and reduced analysis for Joined Wing and a cantilever

For the reduced analysis, the first 60 VMs of the JW is calculated and based on the load 20 most important VMs are chosen

$$\alpha_i = \left| \frac{\phi_i^T \mathbf{f}}{\phi_i^T \mathbf{M} \phi_i} \right| \qquad i = 1 \dots 60 \tag{4.1}$$

where ϕ_is are the first 60 modes, $\mathbf{f}$ and $\mathbf{M}$ denote the external load and the mass matrix respectively. By projecting the load on the VMs, we can find the VMs that the external load strikes mostly. Using the selected VMs, their corresponding MDs are calculated. The reduction basis $\mathbf{\Phi}$ is then made of VMs and MDs. Figure 4.1 shows the solution to the full and reduced analysis. The reduced analysis shown with blue dashed line, does not match the full analysis shown with solid black line. This means that the approximation of the system by the reduced basis is not a good (sufficient) approximation.

4.1.1 Thin cantilever plate

The reduction basis containing VMs and MDs is in this section used for a geometrically simple example namely a simple, thin cantilever plate shown in figure 4.2. It is cantilevered along the line $y = 0$ and the solution is for node with coordinates $[0, 350, 0]$ shown as point G. This structure has the same material properties as the JW and is subjected to a uniform pressure of $P = 2.2050 Kg/(mms^2)$. Because the geometry is

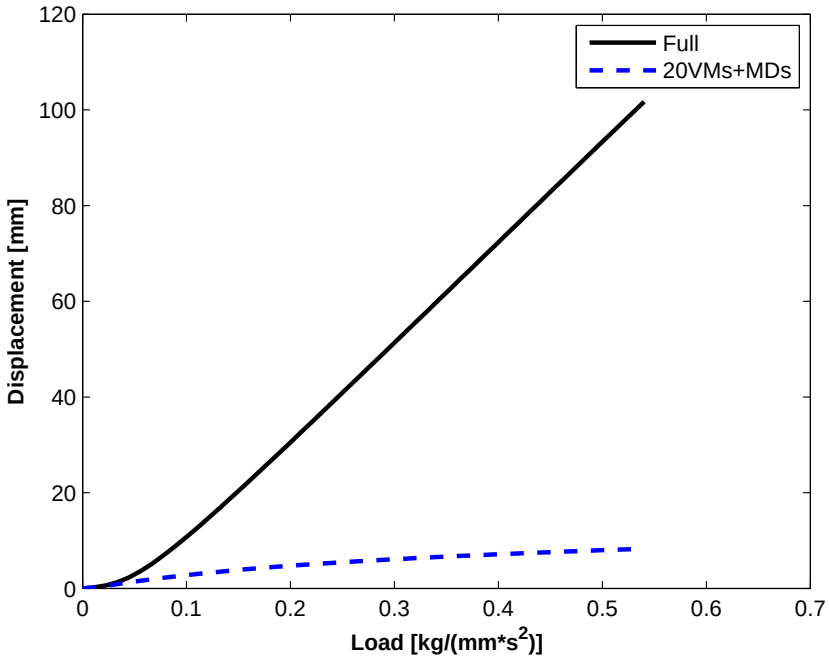

Figure 4.1: The response of the JW full and reduced analysis at point $[50, 500, 0]$ in the vertical direction.

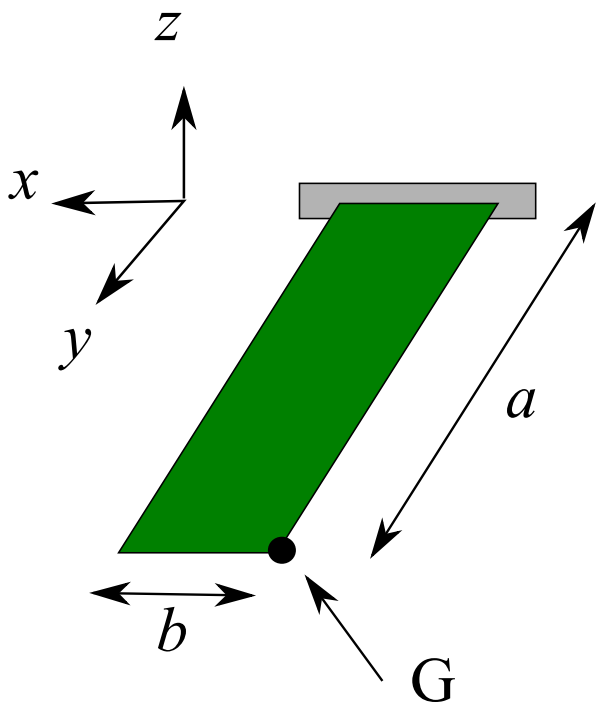

Figure 4.2: Simple thin plate, cantilevered at line $y = 0$. Thickness is $h = 2mm$ and $a = 350mm$ and $b = 50mm$.

simpler than the JW, only 10 most important VMs are selected out of a total 30 VMs calculated. As it can be seen in figure 4.3 the approximation of the system using VMs and MDs is sufficient to approximate the full solution. But by omitting the MDs from the reduction basis, the information in the reduction basis is not sufficient to describe the system.

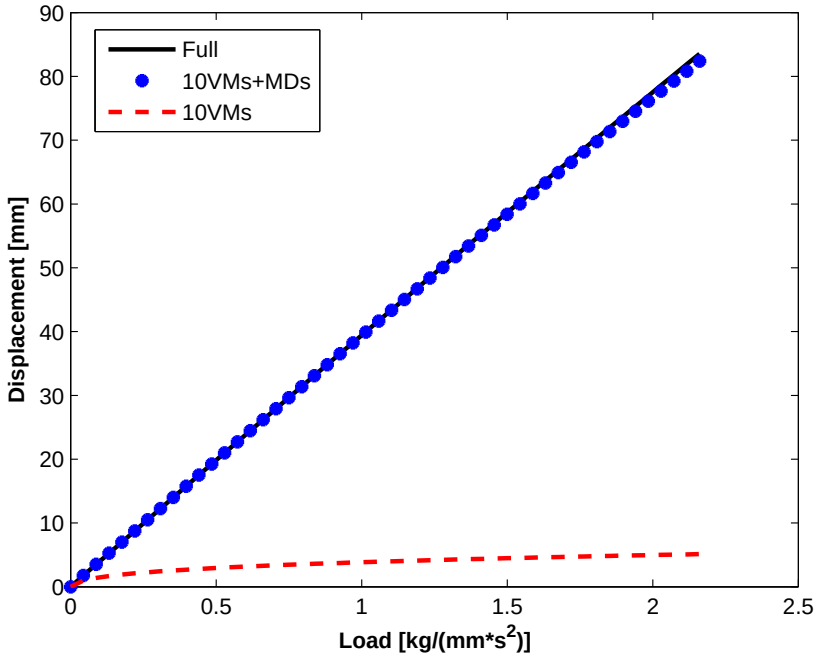

Figure 4.3: The response of a cantilever plate full and reduced analysis at point G in the vertical direction.

Now the question arises that why is it that this approach perfectly reduces the system for a simple cantilever plate but not for the JW? The reason must be in the geometry difference. Taking a look at the JW (Figure 2.4), the flat horizontal plate underneath and the slope plate above it are fixed under two angles around x and z axis. Thus JW is not geometrically symmetric, which could have an influence on the results. In the next section the geometry of the JW will be made simpler and the effect of geometrical symmetry on the effectiveness of the reduction basis will be analysed.

4.2 Symmetric C-shape Structure

In this part the influence of the symmetry of the structure upon the reduction basis is discussed. The structure of the JW has been simplified to a symmetric c-shape structure as in figure 4.4, left hand side. Material properties are the same as introduced in section 4.1. The structure is subjected to a uniform vertical pressure of $P = 0.55125 Kg/(mm.s^2)$.

The thickness of upper and lower plates is $h_1 = 1mm$ and the thickness of the vertical plate is $h_2 = 0.25mm$. To reduce the system, 20 VMs are selected out of 40 VMs and along with their MDs, they form the reduction basis. But the basis is still not rich enough as it can be seen in figure 4.5

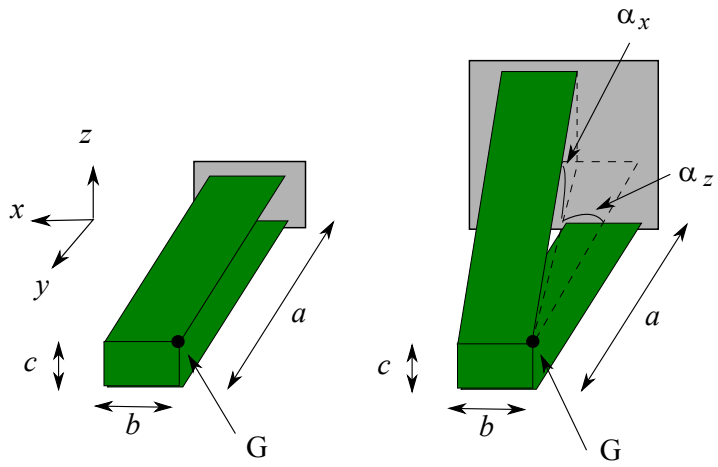

Figure 4.4: Simplification of JW to c-shape. Left: symmetric c-shape; right: asymmetric c-shape. $a = 350mm$, $b = 50mm$ and $c = 20mm$. Solutions found for point G with coordinates $[0, 350, 20]$.

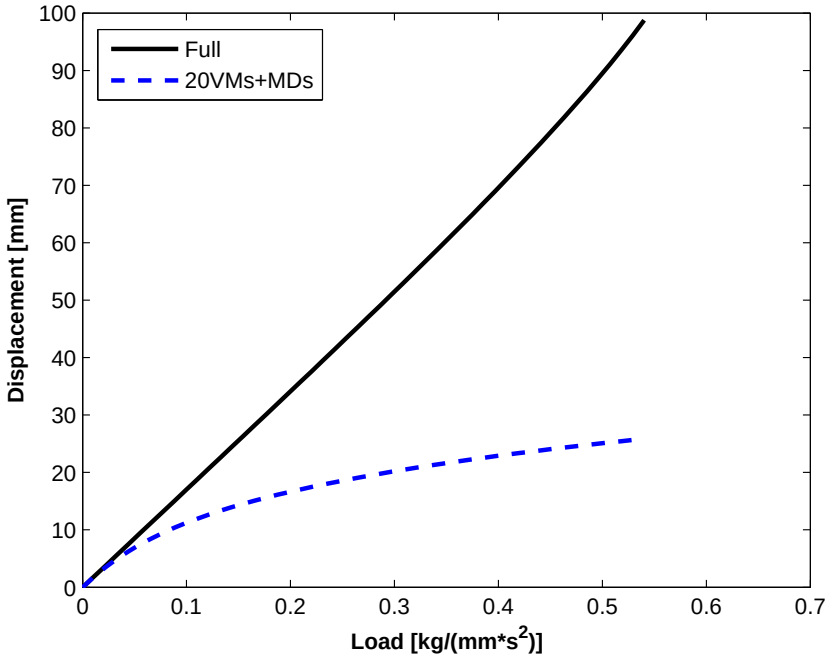

Figure 4.5: The response of a c-shape full and reduced analysis at point $[0, 350, 20]$ in the vertical direction.

4.3 Asymmetric C-shape Structure

In section 4.2 we saw that even for a symmetric c-shape structure, the reduction basis with VMs and MDs, fails to approximate the displacements accurately. Here the symmetric c-shape structure is changed for the upper horizontal plate. This plate is firstly moved with an angle α_x around the x axis. This variation starts with and angle of 0° which corresponds to the symmetric c-shape, to an angle of 6.5° which corresponds to two times the α_x angle of the JW. For the comparison, the displacements calculated with full and reduced analysis at each load step are divided

$$l = \frac{\|\mathbf{u}_{modal}\|}{\|\mathbf{u}_{full}\|} \tag{4.2}$$

and then plotted as a function of $\|\mathbf{u}_{full}\|$. Clearly the ideal line is a constant line $l = 1$. Figure 4.6 shows the comparison with different angles around x axis. The upper

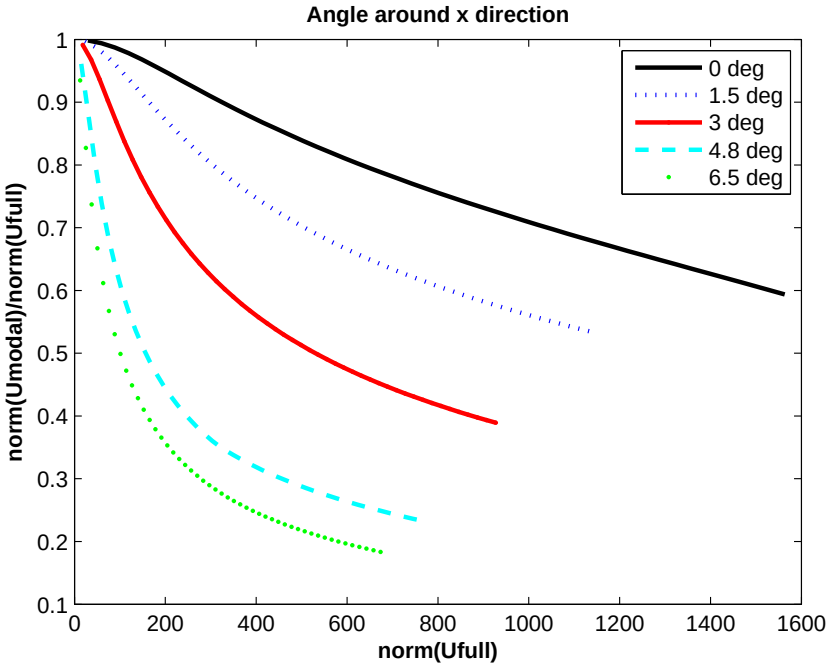

Figure 4.6: Comparison of the results for different angles around x axis.

horizontal plate is then moved with an angle α_z around the z axis between 0° and 15° corresponding to α_z angle of the JW. Results of this comparison are plotted in figure 4.7. Results of angle variation around x and z axis shows that the more symmetric the structure, the more accurate the approximation of displacement by the reduction basis. Thus symmetry can indeed have an influence on the effectiveness of the reduction basis. But even in the best result which is the symmetric c-shape the calculated displacement is not accurate.

For both the JW and the c-shape structures, the vertical plate that joins the other plates together has a small surface are. This makes the stiffness of this plate higher than the rest of the structure. Figure 4.8 shows a triangular c-shape without the vertical plate. As it can be seen in figure 4.9 the approximation of the displacement by the reduction basis is still not accurate.

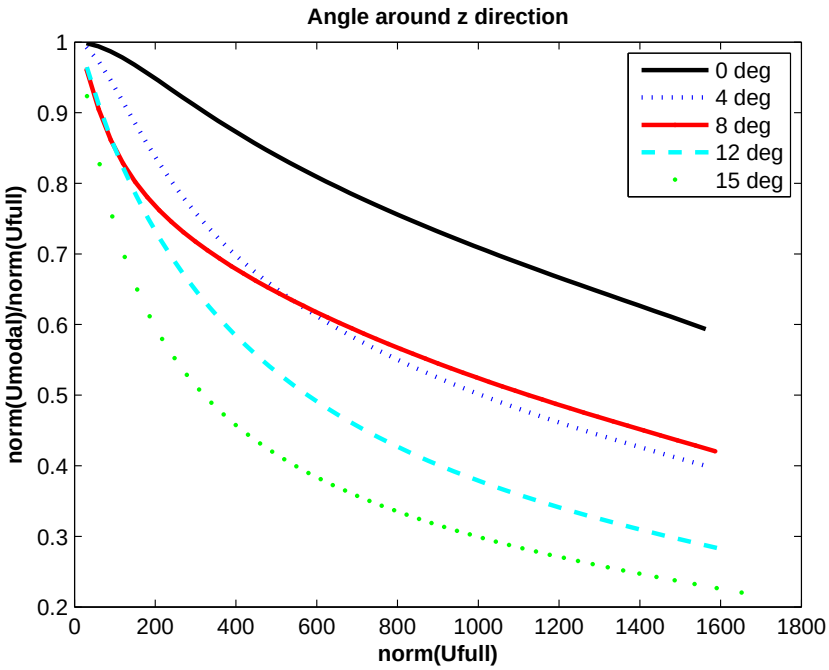

Figure 4.7: Comparison of the results for different angles around z axis.

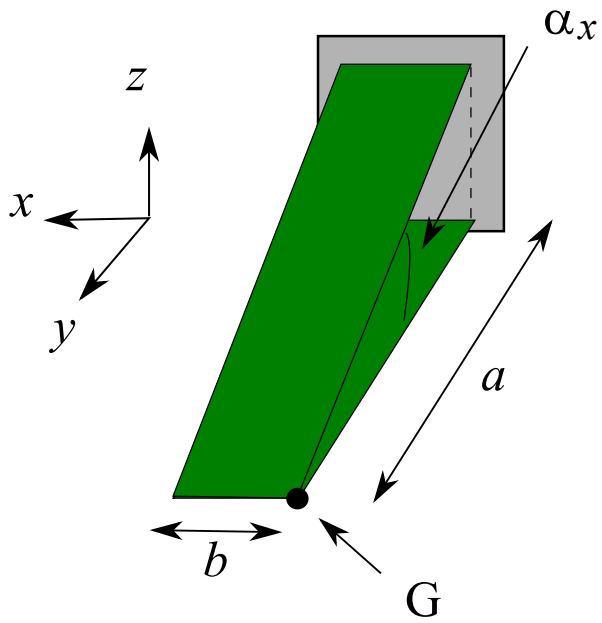

Figure 4.8: Triangular c-shape structure.

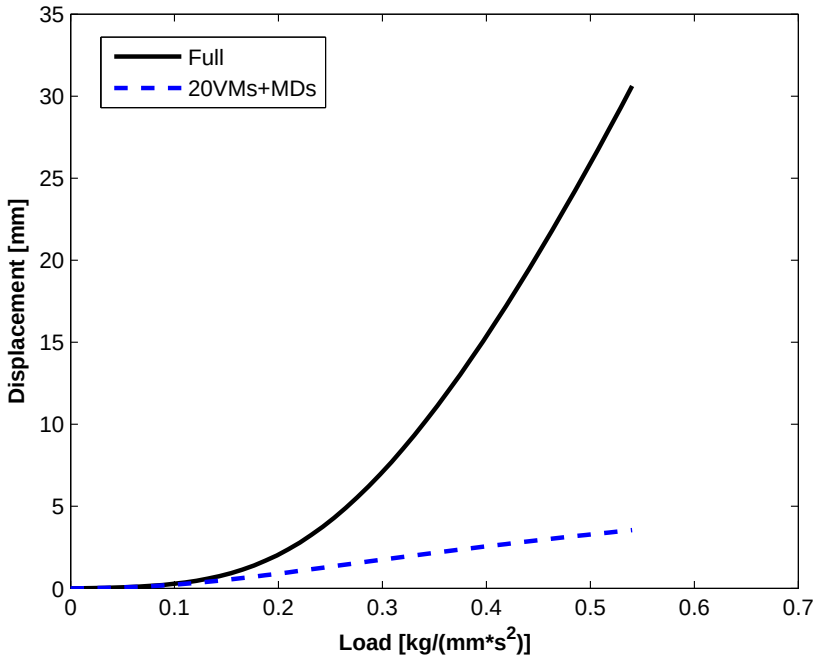

Figure 4.9: Solution of the full and reduced analysis for the triangular c-shape at node G.

For JW the flat horizontal plate underneath and the slope plate above it are flexible structures, because of their rather large surface area and small thickness. But the small vertical plate that joins these two plates is more stiff than the other two due to its geometry. But also the lines that joins the plates form places of high stiffness in the structure. In fact by closely examining the shapes in the reduction basis (figures are included in appendices A and B), one finds out that there are numerous possible deformations of these flexible plates but not very much of the vertical plate and the joining lines. Thus a conclusion is that there is not enough information about this vertical part in the reduction basis. Also because the deformations of this vertical plate are not included in the basis, it restricts the movements of the free end of the structure.

In the next section the remainder is defined and calculated. Intention is to find missing shapes in the reduction basis.

4.4 Remainder

To reduce the system, the displacements are approximated by $\mathbf{u}_{red} = \mathbf{\Phi q}$. This approximation differs from the displacements obtained using the full analysis, by a remainder $\mathbf{r}$

$$\mathbf{u}_{full} = \mathbf{\Phi q} + \mathbf{r} \tag{4.3}$$

where $\mathbf{\Phi}$, is the reduction basis, $\mathbf{q}$ is the vector of modal amplitudes and $\mathbf{r}$ is the remainder (i.e. what is missing in the approximation). Premultiplying this equation with the mass matrix $\mathbf{M}$ and projecting the result on the reduction basis results in

$$\mathbf{\Phi}^T\mathbf{M}\mathbf{u}_{full} = \mathbf{\Phi}^T\mathbf{M}\mathbf{\Phi q} + \mathbf{\Phi}^T\mathbf{M}\mathbf{r} \tag{4.4}$$

if the basis was formed only by VMs, the term $\mathbf{\Phi}^T\mathbf{M}\mathbf{\Phi}$ would have been equal to unity matrix $\mathbf{I}$, but as $\mathbf{\Phi}$ contains also MDs, this matrix is close to $\mathbf{I}$ (i.e. 1s on the diagonal and there are off diagonal terms that are not zero). We call it $\hat{\mathbf{I}}$. The term $\mathbf{\Phi}^T\mathbf{M}\mathbf{r}$ is equal to zero as we impose that the remainder $\mathbf{r}$ produces no work for the assumed modes that are stored in $\mathbf{\Phi}$ [7]. Thus the modal amplitudes can be found and also the remainder

$$\mathbf{q} = \hat{\mathbf{I}}^{-1}\mathbf{\Phi}^T\mathbf{M}\mathbf{u}_{full} \tag{4.5}$$

$$\mathbf{r} = (\mathbf{I} - \mathbf{\Phi}\hat{\mathbf{I}}^{-1}\mathbf{\Phi}^T\mathbf{M})\mathbf{u}_{full} \tag{4.6}$$

where $\mathbf{u}_{full}$ is the matrix of displacement snapshots for the load steps, calculated with the full analysis. The SVD[1] of the remainder shows the most important shapes that $\mathbf{r}$ contains.

For the c-shape, adding the first three important modes to $\mathbf{\Phi}$ results in the response of figure 4.10 (the dotted green line). The new basis perfectly approximates the displacement. These three modes are plotted in figure 4.11 and their side views are shown

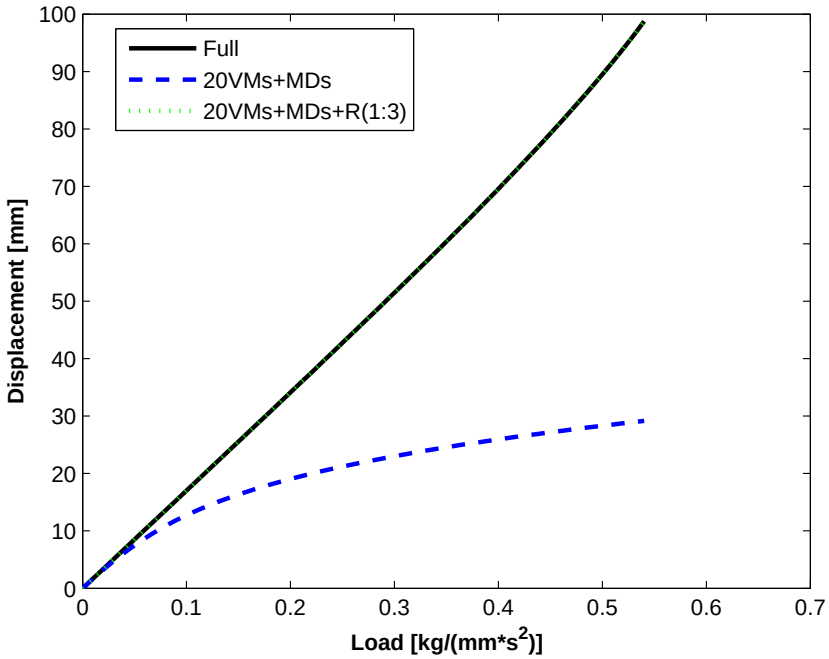

Figure 4.10: The response of the c-shape, full analysis, VM+MD, VM+MD+remainder

in figure 4.12. These modes show a lot of out of plane deformations mostly around the vertical part.

Calculating this remainder for the JW results in the response of figure 4.13 and the first three remainder modes are plotted in figure 4.14. In figure 4.15 the out of plane displacements of these shapes are clearer as it shows the side view of the first three remainder modes.

To see the remainder around the vertical plate, we take a look at the shape of the forces that the remainders produce

$$\mathbf{F} = \mathbf{K}_{lin}\mathbf{r} \tag{4.7}$$

[1]Singular Value decomposition is explained in section 4.5

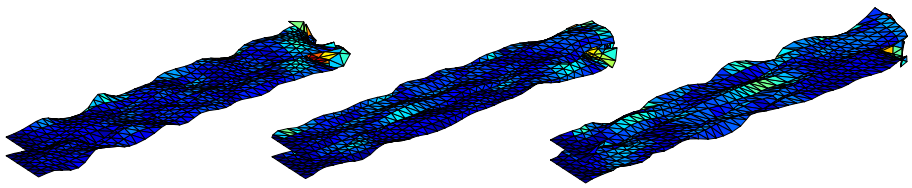

Figure 4.11: The shape of the first three remainder shapes of the c-shape. Left to right is 1 to 3.

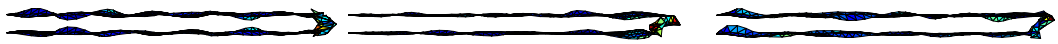

Figure 4.12: The shape of the first three remainder shapes of the c-shape, side view. Left to right is 1 to 3.

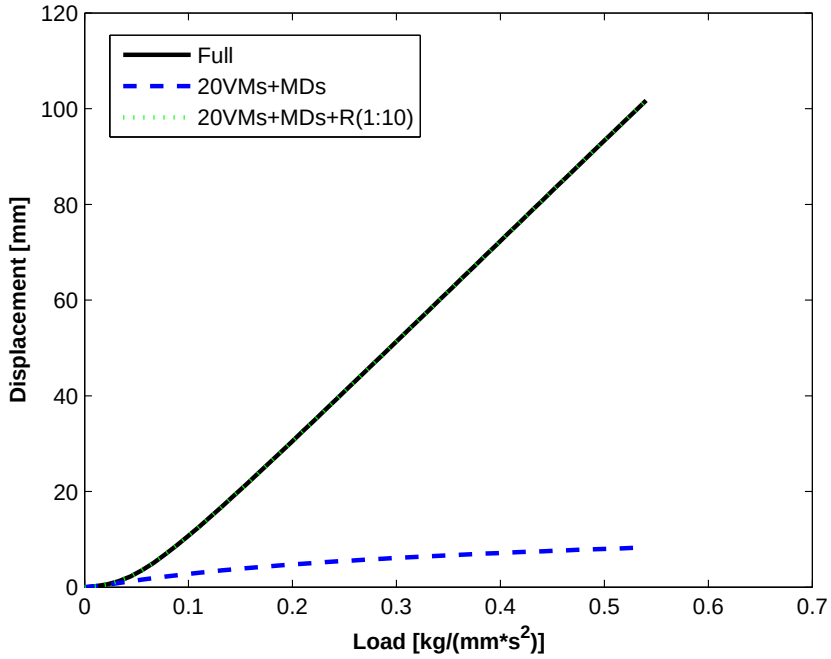

Figure 4.13: The response of the JW, full analysis, VM+MD, VM+MD+remainder

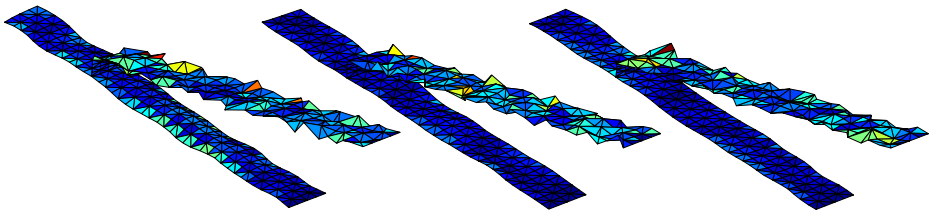

Figure 4.14: The shape of the first three remainder shapes of the JW. Left to right is 1 to 3.

Figure 4.15: The shape of the first three remainder shapes of the JW side view. Left to right is 1 to 3.

These forces are in figure 4.16 for the JW structure. Obviously the out of plane forces and therefore displacements are greater around the vertical plate than elsewhere in the structure.

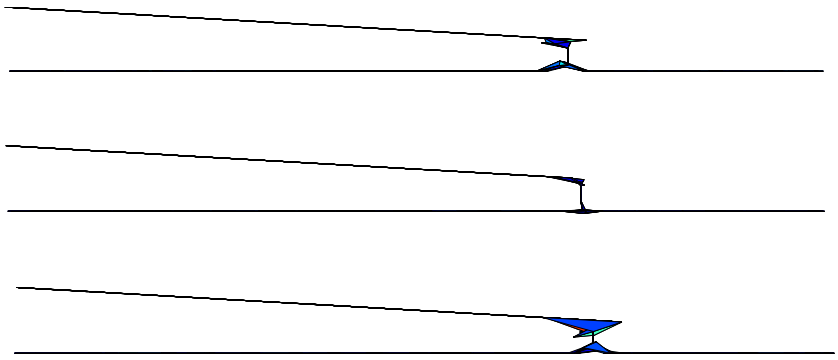

Figure 4.16: The shape of the first three force remainder shapes of the JW side view. Top to bottom is 1 to 3.

4.5 Proper Orthogonal Decomposition

The POD defines a basis for the modal decomposition of set of vectors. These vectors can be experimental data set or a set of numerically generated data as for example displacement snapshots of the JW full analysis response [9].

The idea behind the POD method starts as follows. Assume that you have a series of snapshots of the displacement $\mathbf{u}$ (vector of N long) at several time or load steps $\mathbf{U} = [\mathbf{u}_1, \ldots, \mathbf{u}_k]$. These snapshots span a space $V = \text{span}\{\mathbf{u}_1, \ldots, \mathbf{u}_k\}$. The goal of POD is to find orthonormal vectors $\mathbf{\Psi}_i$, where $i = 1, \ldots, r$, where $r \leq \dim(V)$, such that the $\mathbf{\Psi}_i$ can approximate the space V as effciently as possible. Therefore the following quadratic error is minimized

$$J(\mathbf{\Psi}_1, \ldots, \mathbf{\Psi}_r) = \Sigma_{j=1}^{k} \left| \mathbf{u}_j - \Sigma_{i=1}^{r} (\mathbf{u}_j^T \mathbf{\Psi}_i) \mathbf{\Psi}_i \right|^2 \tag{4.8}$$

given the orthonormality constraint

$$\mathbf{\Psi}_i^T \mathbf{\Psi}_j = \begin{cases} 1 & \text{if} \quad i = j \\ 0 & \text{otherwise} \end{cases} \tag{4.9}$$

It can be shown that this minimisation problem yields the following optimality condition [13]

$$\mathbf{U}\mathbf{U}^T \mathbf{\Psi}_i = \sigma_i^2 \mathbf{\Psi}_i \tag{4.10}$$

where σ_i^2 are the eigenvalues of matrix $\mathbf{U}\mathbf{U}^T$ and the σ_i are the singular values of matrix $\mathbf{U}$. This can be solved by finding the Singular Value Decomposition of the matrix $\mathbf{U}$ with dimensions $[N \times k]$

$$\mathbf{U} = \mathbf{Y}\mathbf{\Sigma}\mathbf{V}^* \tag{4.11}$$

where $\mathbf{V}^*$ denotes a complex conjugate and $\mathbf{\Sigma}$ is a $[N \times k]$ diagonal matrix

$$\mathbf{\Sigma} = \begin{bmatrix} \mathbf{D} & \mathbf{0} \\ \mathbf{0} & \mathbf{0} \end{bmatrix} \tag{4.12}$$

where $\mathbf{D}$ is a $[r \times r]$ diagonal matrix containing the singular values σ_i on its diagonal. Furthermore the singular value decomposition will ensure that [13]

$$\mathbf{U}\mathbf{U}^T \mathbf{Y}_i = \sigma_i^2 \mathbf{Y}_i \tag{4.13}$$

Thus the left singular vectors in $\mathbf{Y}$ form the optimal basis to approximate the space spanned by the snapshots

$$\mathbf{\Psi}_i = \mathbf{Y}_i \tag{4.14}$$

Because the proper orthogonal decomposition $\mathbf{\Psi}$ is tailored to approximate the space spanned by the snapshots, $\mathbf{\Psi}$ forms an ideal basis for non linear model order reduction

$$\mathbf{\Phi} = \mathbf{\Psi} \tag{4.15}$$

The singular values σ_i give the energy stored in the shapes $\mathbf{Y}_i$, therefore the shapes with larger singular values are more important to use in the reduction basis. In this way the most important shapes of the displacement snapshots are used. Figure 4.17 shows modes 3, 4 and 5 of these shapes for the JW.

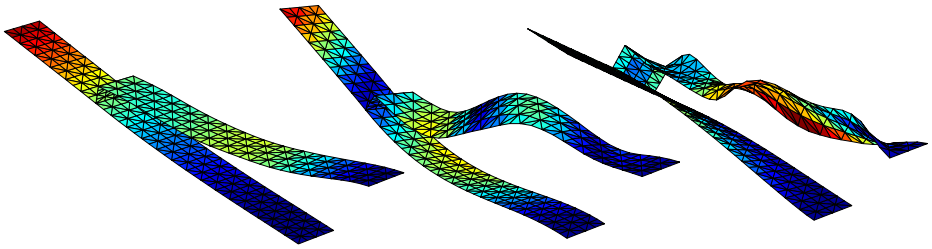

Figure 4.17: Shapes 3,4 and 5 of most important shapes of the POD of the full analysis displacement snapshots.

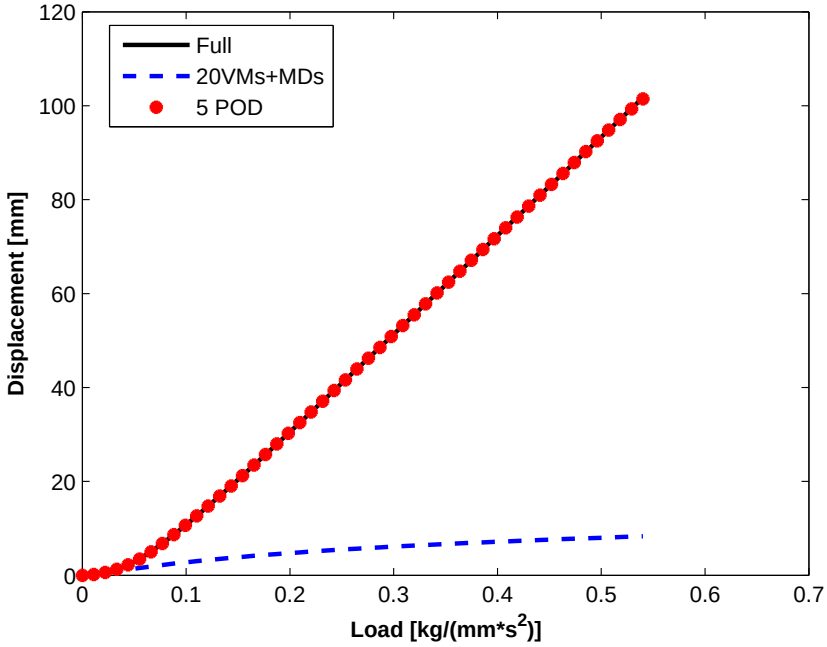

Figure 4.18: The response of the JW, using 5 POD modes in the reduction basis.

Figure 4.18 shows the response of the JW using only first 5 POD modes in the reduction basis. The response using POD modes in the reduction basis perfectly matches the full analysis.

Although using the SVD modes of the remainder or POD modes of the full analysis displacement snapshots in the basis can reduce the system perfectly, there is the disadvantage that still results of the full analysis are needed to build the basis. While the goal is to reduce the system in such a way that there is no need for the full analysis.

4.6 Wilson vectors of the remainder (Krylov sequence)

Krylov sequence is a mathematical iterative method to generate vectors that can approximate the system. Normally it is a cheap method to find vectors for the reduction basis that resemble vibration modes [2]. In this method sequential vectors are found starting with a displacement and using the mass matrix $\mathbf{M}$ and static stiffness matrix $\mathbf{K}$. These vectors are then orthogonalized and mass normalized.

$$\mathbf{W} = [\mathbf{u}_1, \mathbf{u}_2, \ldots, \mathbf{u}_n] \tag{4.16}$$

$$\mathbf{W} = [\mathbf{u}_1, \mathbf{K}^{-1}\mathbf{M}\mathbf{u}_1, \ldots, \mathbf{K}^{-1}\mathbf{M}\mathbf{u}_{n-1}] \qquad i = 1 \ldots n \tag{4.17}$$

where the starting vector $\mathbf{u}_1$ and the number of generated vectors can be chosen. That the results of this scheme resemble eigenmode shapes can be seen by the similarity of this algorithm to a power iteration eigenvalue scheme.

The physical meaning of $\mathbf{u}_i$, can be seen by considering $\mathbf{M}\mathbf{u}_{i-1}$, which gives the force due to an acceleration $\mathbf{u}_{i-1}$. The resulting elastic displacement $\mathbf{u}_i$ is then equal to $\mathbf{K}^{-1}$ times this force.

In our case the first vector $\mathbf{u}_1$ will be the first SVD vector of the set of remainder snapshots as discussed in section 4.4 and 2 additional vectors from the Wilson sequence are calculated (total of three vectors). The modal derivatives of these Wilson vectors and the VMs are calculated and the reduction basis is formed with VMs, MDs of VMs and Wilson vectors and MDs of Wilson vectors. As the basis contains the most important shape of the remainder, it is expected that the reduction basis is rich enough to approximate the full system. And figure 4.19 shows that the approximation is improved using Wilson vectors. Furthermore figure 4.20 shows shapes of the three Wilson vectors. It can be seen that they contain higher bending modes and in-plane effects that obviously can not exist in the lower eigenmodes (VMs).

A disadvantage of the method is that also in this case the full analysis is needed to build the reduction basis. The full analysis is needed because the SVD of the remainder snapshots obtained from a full analysis is used to start the Krylov sequence.

4.7 Greedy Algorithm

Greedy algorithm is an optimisation algorithm which is used here to optimise the reduction basis. This algorithm looks for the best possible enrichment in each increment

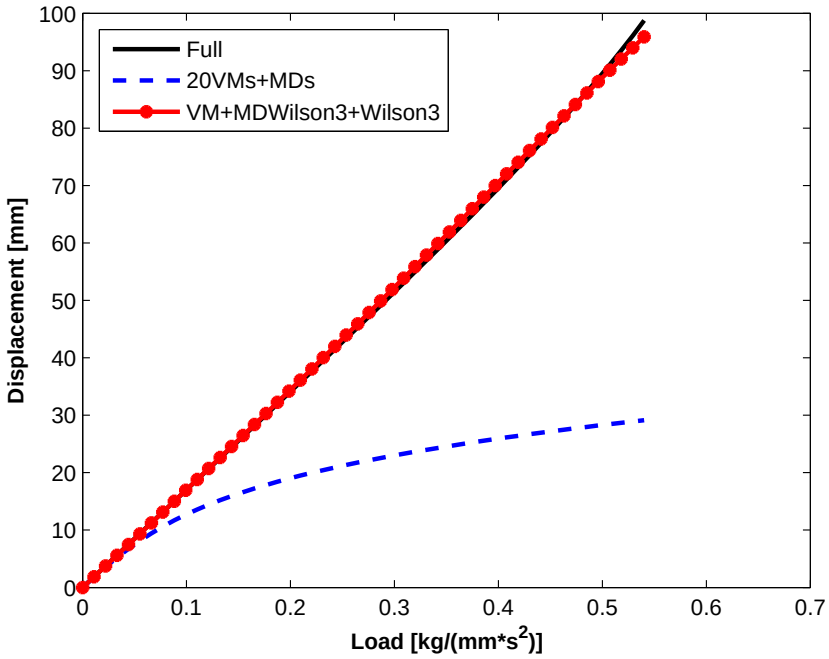

Figure 4.19: The response of the c-shape structure, using Wilson vectors and their modal derivatives in the reduction basis.

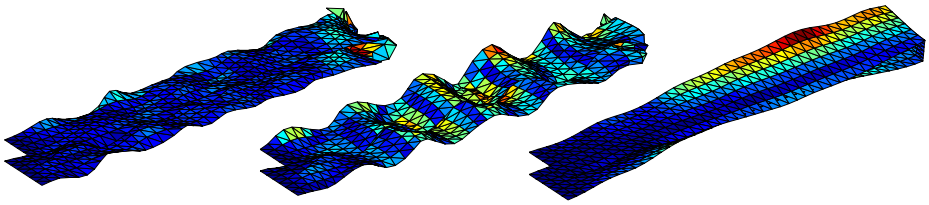

Figure 4.20: Three Wilson vectors calculated from the remainder of the c-shape.

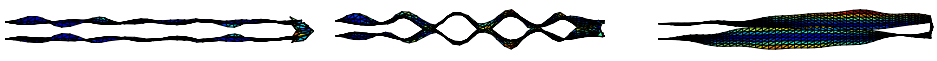

Figure 4.21: Three Wilson vectors calculated from the remainder of the c-shape side view.

in the hope to obtain the best possible response for the whole set of increments [4]. We start with the reduction basis $\mathbf{\Phi}$ containing vibration modes and modal derivatives. Using this basis we can solve for the first load step and obtain the modal amplitudes $\mathbf{q}$. The approximate displacement for the first increment is then

$$\mathbf{u}^i = \mathbf{\Phi}^i \mathbf{q}^i \tag{4.18}$$

which results in $\mathbf{f}_{int}(\mathbf{u}) = \mathbf{f}_{int}(\mathbf{\Phi q})$. Because the displacement is approximated by $\mathbf{\Phi q}$ and thus is not the displacement obtained by the full analysis, the internal force is not equal to the external force. This enables the definition of the residual at load step i

$$\mathbf{e}^i = \mathbf{f}^i_{int}(\mathbf{\Phi q}^i) - \mathbf{f}^i_{ext} \tag{4.19}$$

Therefore the force error at load step i can be defined as

$$e^i = \frac{\|\mathbf{f}^i_{int} - \mathbf{f}^i_{ext}\|}{\|\mathbf{f}^i_{ext}\|} \tag{4.20}$$

where i denotes the increment number (load step). If the error is greater than a specific value, the greedy algorithm uses the residual $\mathbf{e}^i$ to generate Wilson vectors and adds these vectors together with their modal derivatives and VMs to the reduction basis. The increment is solved again until the error value drops to the set value. In this way the greedy algorithm optimises the reduction basis by finding the best (using the residual of that increment) possible Wilson vectors for an increment. The flowchart of the greedy algorithm is in figure 4.22.

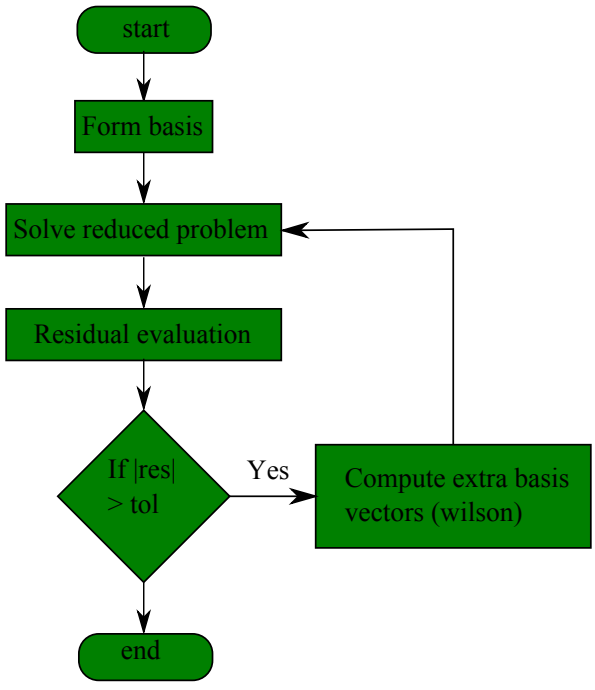

Figure 4.22: Flowchart of the greedy algorithm.

As a short example the linear case is analysed

- using the reduction basis the stiffness matrix and the load vector are reduced

$$\tilde{\mathbf{K}} = \mathbf{\Phi}^T \mathbf{K} \mathbf{\Phi} \qquad \tilde{\mathbf{f}}_{ext} = \mathbf{\Phi}^T \mathbf{f}_{ext} \tag{4.21}$$

- the modal amplitudes and the displacement approximation are calculated

$$\mathbf{q} = \tilde{\mathbf{K}}\tilde{\mathbf{f}}_{ext} \qquad \mathbf{u} = \mathbf{\Phi q} \tag{4.22}$$

- now the internal force $\mathbf{f}_{int}$ is

$$\mathbf{f}_{int} = \mathbf{K\Phi q} \tag{4.23}$$

  as it is a linear case, the solution is exact and no more than one increment (namely the last increment) is needed. So the difference between the internal load found by the approximation, and the external load is

$$\mathbf{e} = \mathbf{f}_{int} - \mathbf{f}_{ext} \tag{4.24}$$

  and by adding the displacement resulted from this force difference $\mathbf{e}$ to the reduction basis, the exact solution is found.

In other words, we want to solve the equation

$$\mathbf{Ku} = \mathbf{f}_{ext} \tag{4.25}$$

in the linear case, given the stiffness matrix and the external load vector. As there are a large number of DoFs, we want to reduce the system, so an approximation for $\mathbf{u}$ is

$$\mathbf{u} = \mathbf{\Phi q} \tag{4.26}$$

introducing equation 4.26 in equation 4.25

$$\mathbf{K\Phi q} = \mathbf{f}_{ext} + \mathbf{e} \tag{4.27}$$

Now assume that there exists a displacement ϕ_{Greedy} that when multiplied by the stiffness matrix, results in the residual force vector

$$\mathbf{K}\phi_{Greedy} = \mathbf{r} \qquad \Rightarrow \qquad \phi_{Greedy} = \mathbf{K}^{-1}\mathbf{e} \tag{4.28}$$

The basis takes the form

$$\mathbf{\Phi}_{new} = [\mathbf{\Phi}_{old} \qquad \phi_{Greedy}] \tag{4.29}$$

In the linear case ϕ_{Greedy} gives the exact solution and $\mathbf{e}$ is calculated exactly.

It is interesting to see the so called static mode $\mathbf{x}_{st}$

$$\mathbf{x}_{st} = \mathbf{K}^{-1}\mathbf{f}_{ext} \tag{4.30}$$

which after orthogonalisation to the basis is equal to

$$\mathbf{x}_{st,orth} = \mathbf{K}^{-1}\mathbf{e} \tag{4.31}$$

Therefore in the linear case the extra basis vector ϕ_{Greedy} is in that case equal to the so called static mode.

In the nonlinear greedy case the for each increment first the displacement is computed with the original basis. Then the $\mathbf{f}_{int}$ is calculated, this gives $\mathbf{e}$. If the error is greater than a set value the wilson sequence is calculated where the starting vector of the wilson sequence $\mathbf{u}_1$ at increment i is equal to the orthogonalized static mode

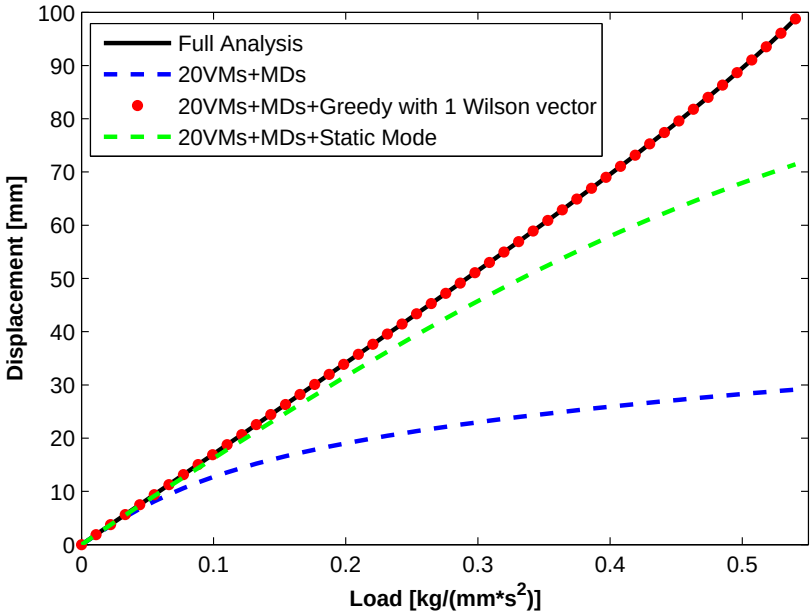

Figure 4.23: The result of the greedy algorithm for the c-shape.

computed with $\mathbf{K}_{tan}$ at the increment i.

The algorithm is used to reduce the basis of the c-shape structure. Figure 4.23 shows that the algorithm gives a good result, it also shows that only adding the static mode for the $\mathbf{u} = \mathbf{0}$ equilibrium to the initial reduction basis, without basis updating already improves the result significantly

The algorithm is used to reduce the basis of the JW. Figure 4.24 shows that the algorithm gives a good result, it also shows that only adding the static mode for the $\mathbf{u} = \mathbf{0}$ equilibrium to the initial reduction basis, without basis updating in this case does not significantly improve the result. One reason for this is that the c-shape behaviour is closer to linear behavior as the JW behaviour. The greedy algorithm only needed to compute a Wilson vector about 8 times.

The advantage of the greedy algorithm is that the results of the full analysis are not needed anymore.

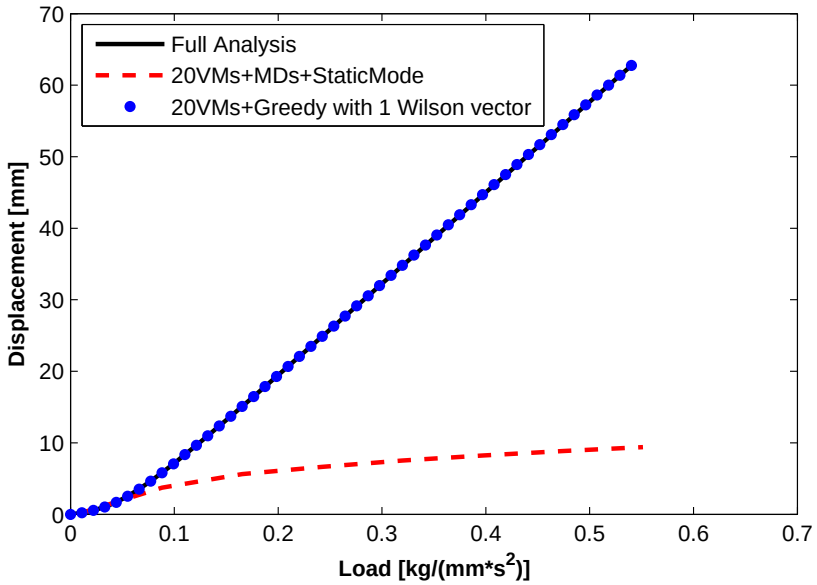

Figure 4.24: The result of the greedy algorithm for the JW.

Chapter 5

Discussion

In the previous chapter different methods where discussed in order to enrich the reduction basis for the JW structure.

First the simple cantilever is discussed. For this structure the use of VMs and MDs in the reduction basis, perfectly approximates the displacement. Afterwards the c-shape structure is introduced and the influence of the symmetry of the structure on the effectiveness of the reduction basis is analysed. Although symmetry is advantageous for the effectiveness of the reduction basis, the work of the reduction basis in approximating the displacement is still poor. The expectation is that the reduction basis lacks flexible displacement shapes around joins of the structure.

We looked at the set of remainders of the reduction basis. The set of remainders contains the remainders of the reduction basis at each increment. A remainder 'contains' the mode shape that, for that increment, is missing from the reduction basis constructed out of VMs and MDs. The shapes of the remainder shows indeed lots of out of plane displacements around the joining lines with the vertical plate. The most important shapes that captures the data for all increments into one shape can be computed using SVD. Including this most important shapes into the reduction basis resulted in a basis that could perfectly approximate the system. The disadvantage of this method is that it needs the results of the full analysis, while the goal is to enrich the basis in a way that the full analysis is not needed anymore.

Also the POD method is discussed, in this method the displacement snapshots (for the load steps) are used to construct the reduction basis. Calculating the SVD of the snapshots gives the shapes that contain the most energy values. This gives the opportunity to construct the basis with a small number of modes, while the reduction basis containing VMs and MDs had at least hundreds of modes. Again a disadvantage is that the POD method needs the results of the full analysis. However using POD might give the possibility to find the right enrichment to use for dynamic analysis. Another theoretical option would be to extrapolate the results of the static analysis to large loads, although this was proven to be not very effective by [5].

The method of Wilson vectors is an efficient, computationally cheap method to calculate for a set of shapes that can be used to fill a base, e.g. a reduction base. They work well because Wilson's method resembles the power iteration method for

eigenvalue computation.

But in a nonlinear case like the JW, the starting point to calculate the Krylov sequence is crucial. As it was discussed that the eigenmodes of the nonlinear structure change with different load steps, as the stiffness matrix and the geometry of the structure change rigorously. Using the results of the full analysis, in this case the most important remainder, gives good initial vectors to start the Krylov sequence and gives good results for the c-shape.

Comparing the important shapes extracted using these methods, with VMs and MDs of the JW structure (appendices A and B) we see a lot of out of plane displacements around the joining lines with the vertical plate. This part is geometrically very different than the rest of the JW structure and therefore its stiffness is greater than the other two plates it joins.

Also a lot of in plane deformations can be seen for the slope plate of the JW. For the simple cantilever structure, MDs contain a lot of in plane information, which helps enriching the reduction basis very cheaply and efficiently. But for the JW structure the MDs can not fully describe the in plane deformations of the structure.

Therefore one idea can be to use substructuring methods such as Craig-Bampton to analyse different plates of the structure separately. Another idea is to look at higher order modal derivatives, to see whether the missing information can be found in there.

The greedy algorithm searches for the best possible enrichment of the basis at each load step, with the expectation that the final overall result will also be the best. Which indeed gives a very good result both for the c-shape and the JW. This method is mostly advantageous in comparing with methods mentioned before, because it does not need the results of the full analysis. However the effectiveness of the algorithm was highly sensitive to the error tolerance used to decide whether to update the basis or not.

For any thin walled structure in plane deformations will create very high in plane internal forces. These high internal forces do not influence the out-of plane result too much, however they do influence the norm of the error estimate. This influence on the error estimate makes the choice of a Greedy tolerance especially difficult.

Chapter 6

Conclusions and recommendations

The goal of this project was to find out why modal order reduction using VMs and MDs fails to approximate the displacement for the reduced JW problem.

The reduction basis with VMs and MDs works perfectly for the problem of a simple cantilever. For this structure the MDs show in plane deformations. However for more complex structures such as c-shape and JW, this method fails because of geometrical asymmetry of the structure and plates with high stiffnesses. Also the joins of the plates together, form areas with higher stiffness.

POD method and the method of Wilson vectors can enrich the reduction basis in order to obtain results that approximate the displacements accurately. However these methods need the results of the full analysis, which is a disadvantage. An alternative is to use the greedy algorithm.

The greedy algorithm works for all situations presented in this work. By tuning the error tolerance also better convergence times can be achieved. The results obtained by greedy algorithm can fully describe the reduced system and can be used to investigate the model of JW dynamically. Thus from the methods tested in this report, greedy is optimal.

It is recommended to test other methods for model order reduction of JW as well. The reduction basis obtained by greedy algorithm can fully describe the reduced system and can be used to investigate the model of JW dynamically.

The modal order reduction for a nonlinear structure such as JW can also be done using nonlinear substructuring methods. One such method is the Craig-Bampton method. In this way the stiffnesses and out of plane deformations that occur at the joining lines could be less effective.

If the structure is to be investigated not as substructures, including higher order modal derivatives could add more information to the reduction basis.

Appendix A

First 24 VMs of JW

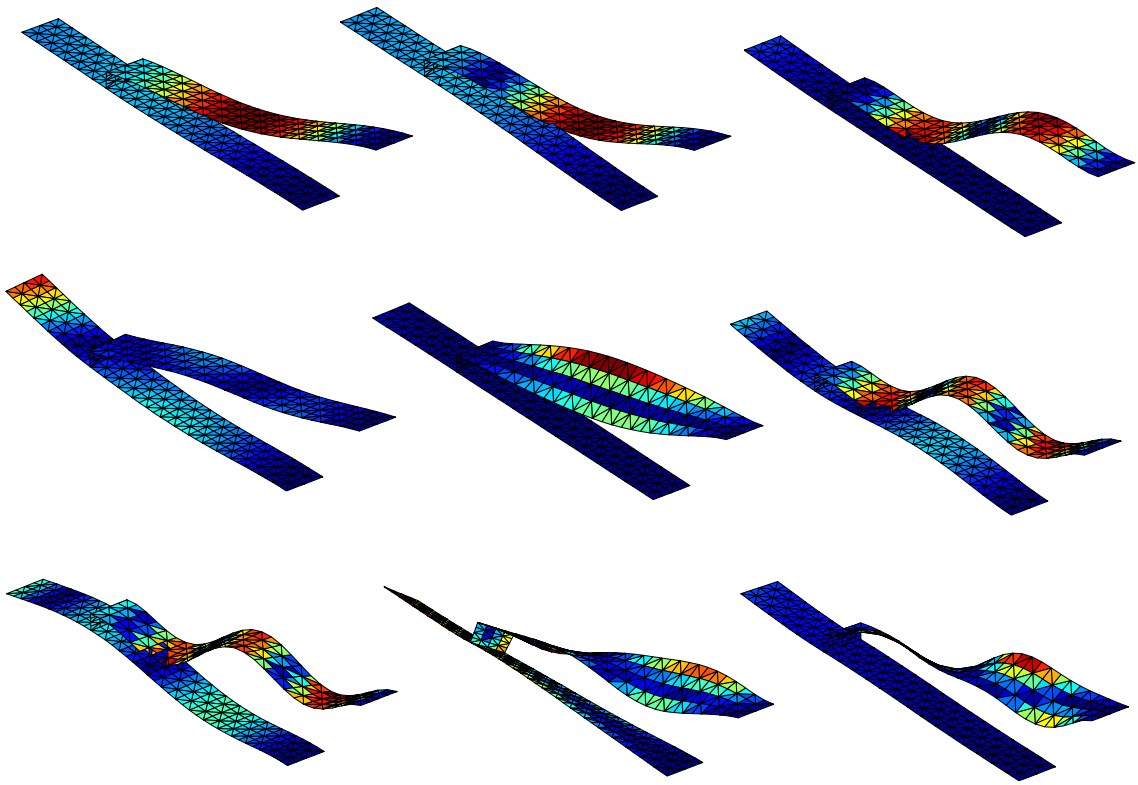

Figure A.1: First 9 VMs of the JW.

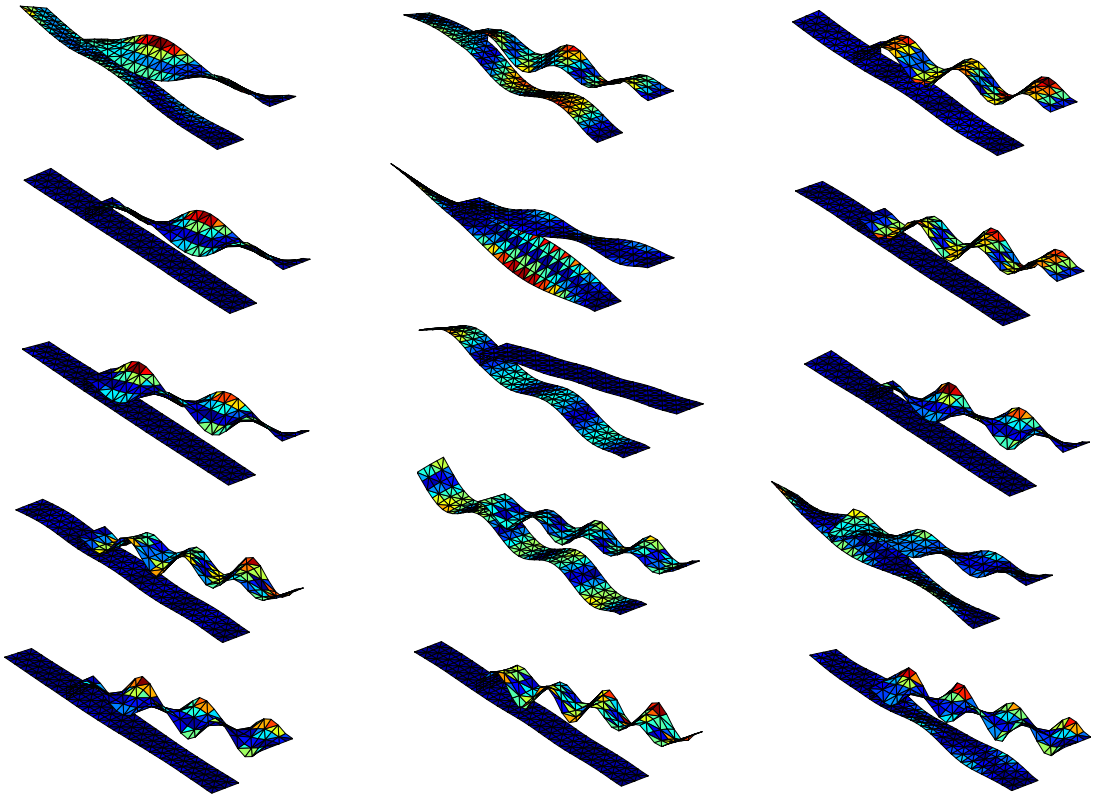

Figure A.2: VMs 10 to 24 of the JW.

Appendix B

First 24 most important MDs of JW

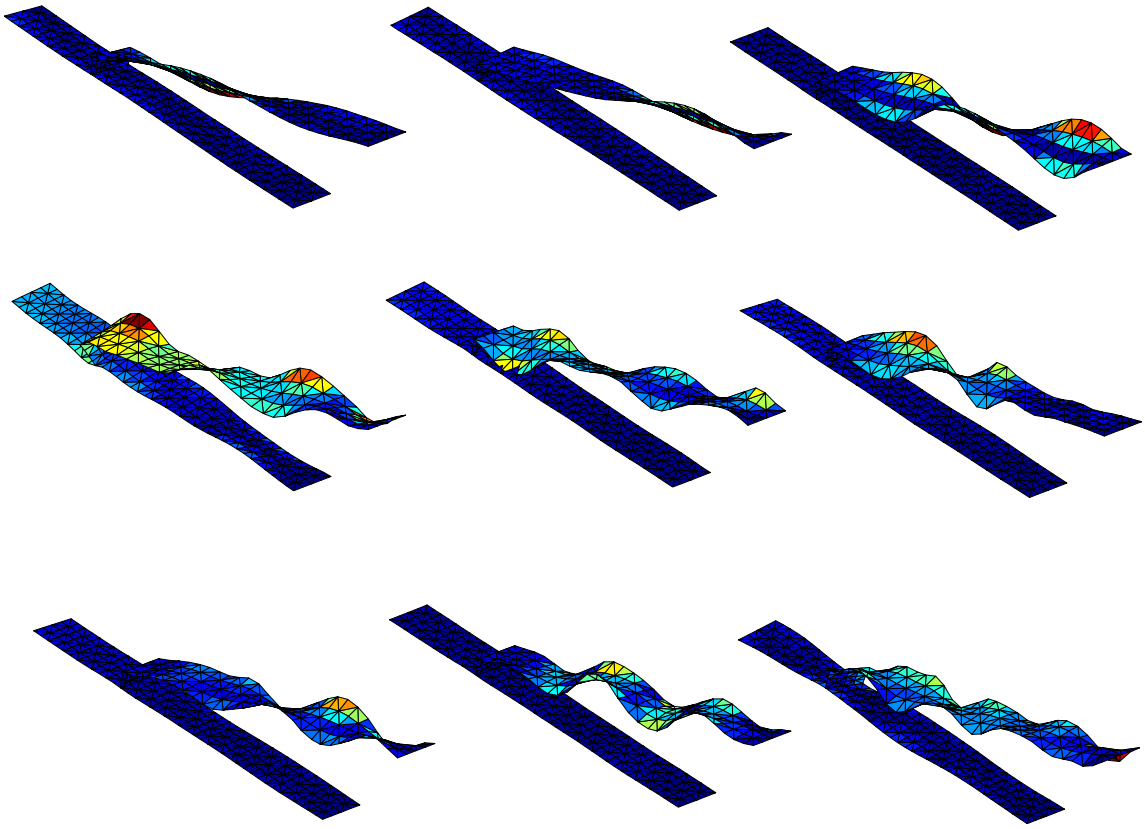

Figure B.1: First 9 important MDs of the JW. Obtained by taking SVD of the MDs

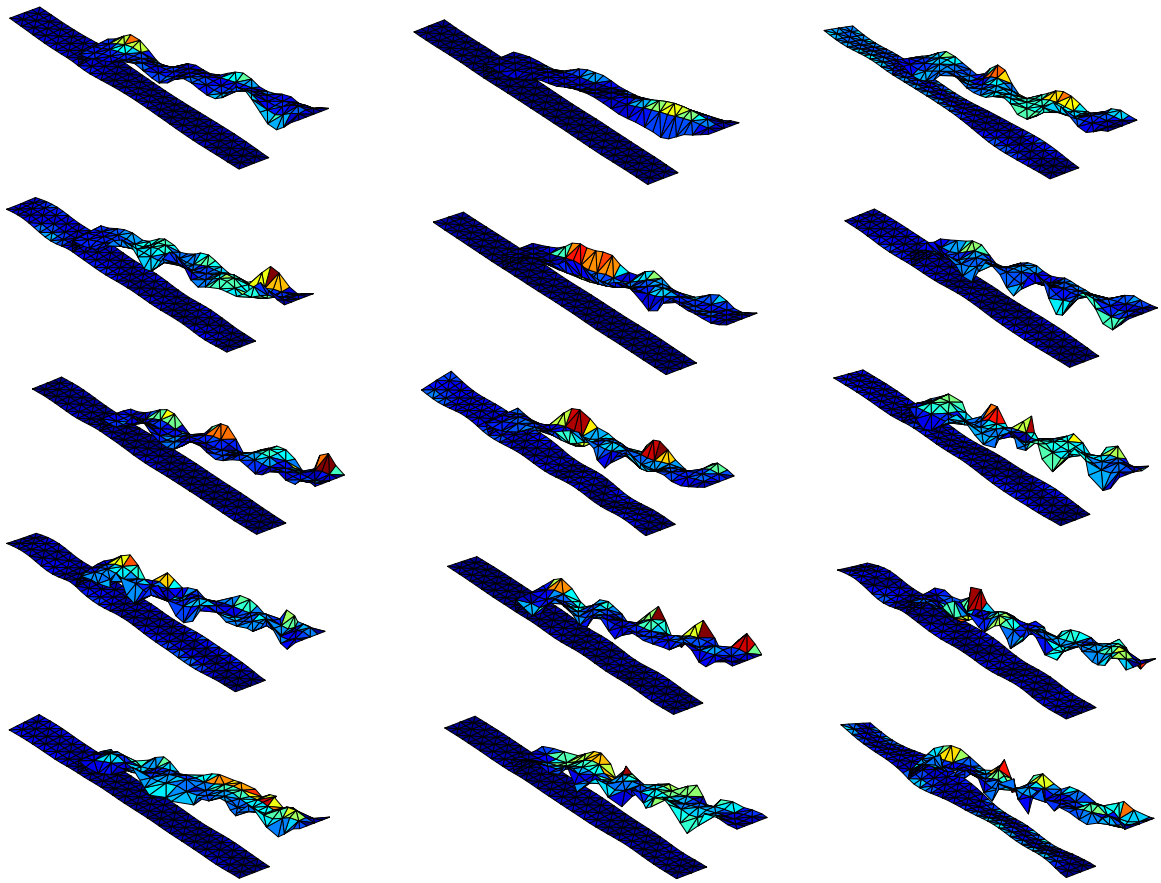

Figure B.2: Important MDs of the JW 10 to 24. Obtained by taking SVD of the MDs

Bibliography

[1] K.J. Bathe. *Finite element procedures*, volume 2. Prentice hall Englewood Cliffs, NJ, 1996.

[2] K.S. Carney. *Improvements in block-Krylov Ritz vectors and the boundary flexibility method of component synthesis*. PhD thesis, Case Western Reserve University, 1997.

[3] E.G. Carnoy. Asymptotic study of the elastic postbuckling behavior of structures by the finite element method. *Computer Methods in Applied Mechanics and Engineering*, 29(2):147–173, 1981.

[4] T.H. Cormen. *Introduction to algorithms*. The MIT press, 2001.

[5] L. Demasi and A. Palacios. A reduced order nonlinear aeroelastic analysis of joined wings based on the proper orthogonal decomposition. *51th AIAA/ASME/ASCE/AHS/ASC Structures, Structural Dynamics, and Materials Conference*, 2010.

[6] MJ Fagan. *Finite element analysis: theory and practice*. 1992.

[7] M. Géradin and D. Rixen. *Mechanical vibrations: theory and application to structural dynamics*. Wiley, 1997.

[8] SDA Hannot and DJ Rixen. Building and reducing a three-field finite-element model of a damped electromechanical actuator. *Microelectromechanical Systems, Journal of*, 20(3):665–675, 2011.

[9] G. Kerschen, J. Golinval, A.F. Vakakis, and L.A. Bergman. The method of proper orthogonal decomposition for dynamical characterization and order reduction of mechanical systems: an overview. *Nonlinear Dynamics*, 41(1):147–169, 2005.

[10] I. Kroo. Nonplanar wing concepts for increased aircraft efficiency. *VKI lecture series on Innovative Configurations and Advanced Concepts for Future Civil Aircraft*, 2005.

[11] I Kroo, J McMasters, and S.C. Smith. Highly nonplanar lifting systems. *Transportation Beyond 2000: Technologies Needed for Engineering Design*, 1995.

[12] C. Lanczos. *The variational principles of mechanics*. Number 4. Dover Pubns, 1970.

[13] YC Liang, HP Lee, SP Lim, WZ Lin, KH Lee, and CG Wu. Proper orthogonal decomposition and its applications–part i: Theory. *Journal of Sound and Vibration*, 252(3):527–544, 2002.

[14] PMA Slaats, J. De Jongh, and A. Sauren. Model reduction tools for nonlinear structural dynamics. *Computers & structures*, 54(6):1155–1171, 1995.

[15] P. Tiso. *Finite element based reduction methods for static and dynamic analysis of thin-walled structures*. PhD thesis, Delft University of Technology, 2006.

[16] P. Tiso. Optimal second order reduction basis selection for nonlinear transient analysis. *Modal Analysis Topics, Volume 3*, pages 27–39, 2011.

[17] F. Van Keulen and H. De Boer. Rigorous improvement of semi-analytical design sensitivities by exact differentiation of rigid body motions. *International journal for numerical methods in engineering*, 42(1):71–91, 1998.

[18] J. Wolkovitch. The joined wing-an overview. 1986.